Norwegian Meteorological Institute

METreport

No. 05/2024
ISSN 2387-4201
Meteorology

# Enhancing hourly precipitation estimates: Addressing wind-induced loss in the combination of modelled and observed data

Cristian Lussana

The Norwegian Meteorological Institute, Oslo, Norway

Norwegian Meteorological Institute

# METreport

| Title | Date |
|---|---|
| Enhancing hourly precipitation estimates: Addressing wind-induced loss in the combination of modelled and observed data | April 15, 2024 |
| **Section** | **Report no.** |
| Division for Climate Services | 05/2024 |
| **Author(s)** | **Classification** |
| Cristian Lussana | ● Free ○ Restricted |


**Abstract**

In-situ hourly precipitation observations often underestimate actual surface precipitation. When integrated with model fields in spatial precipitation analyses, this underestimation can significantly affect monthly or annual aggregations, crucial for calibrating hydrological models. To address this, correction methods utilizing temperature and wind speed have been developed. This study employs corrections using 2m temperature and 10m wind speed from model outputs, assessing their impact on observed data. Since in-situ observations are considered the most accurate data source for hourly precipitation, the question of an appropriate reference for evaluating the quality of the corrections is raised. Here, we use mean annual precipitation from model outputs as a reference, suitable for the objectives of our study. Our findings indicate that applying the proposed corrections more closely aligns observed data with model predictions.



**Keywords**

Hourly Precipitation, Precipitation correction, Snow, Rain, Norway, NORA3, MET Nordic, Rain gauges


| Disciplinary signature | Responsible signature |
|---|---|
| Hans Olav Hygen | Cecilie Stenersen |


**Norwegian Meteorological Institute**
Org.no 971274042
post@met.no
www.met.no / www.yr.no

**Oslo**
P.O. Box 43, Blindern
0313 Oslo, Norway
T. +47 22 96 30 00

**Bergen**
Allégaten 70
5007 Bergen, Norway
T. +47 55 23 66 00

**Tromsø**
P.O. Box 6314, Langnes
9293 Tromsø, Norway
T. +47 77 62 13 00

# Contents

# 1 Introduction

Measurements of precipitation recorded by automatic weather stations are often lower than the actual amounts of precipitation. This underestimation is more pronounced for solid precipitation compared to liquid precipitation and it is influenced by wind, temperature conditions and precipitation intensity.
According to *WMO-No.8* (2021) Sec. 6.4 "Precipitation gauge errors and corrections":

> The true amount of precipitation may be estimated by correcting for some or all of the various error terms listed below:
>
> (a) Error due to systematic wind field deformation above the gauge orifice: typically 2% to 10% for rain and 10% to 50% for snow;
>
> (b) Error due to the wetting loss on the internal walls of the collector;
>
> (c) Error due to the wetting loss in the container when it is emptied: typically 2% to 15% in summer and 1% to 8% in winter, for (b) and (c) together;
>
> (d) Error due to evaporation from the container (most important in hot climates): 0% to 4%;
>
> (e) Error due to blowing and drifting snow;
>
> (f) Error due to the in- and out-splashing of water: 1% to 2%;
>
> (g) Systematic mechanical and sampling errors, and dynamic effects errors (i.e. systematic delay due to instrument response time): typically 5% to 15% for rainfall intensity, or even more in high-rate events;
>
> (h) Random observational and instrumental errors, including incorrect gauge reading times.
>
> The first seven error components are systematic and are listed in order of general importance. The net error due to blowing and drifting snow and to in- and out-splashing of water can be either negative or positive, while net systematic errors due to the wind field and other factors are negative.

In the work by *Pollock et al.* (2018), they concluded that:

> Systematic bias caused by wind is inherent within rainfall measurements and wind is therefore the most important variable required to understand the extent of undercatch on rainfall measurements.

The study by *Pollock et al.* (2018) focused on liquid precipitation employing pit gauges as reference instruments at two locations in the United Kingdom. It quantitatively assessed the undercatch,

which was influenced by factors such as the exposure of the site, the height at which measurements were taken, and the aerodynamic design of the rain gauge. At a low-land site with good exposure and comparatively lower average wind speeds, the observed range of mean undercatch for a standard cylindrical gauge positioned 0.5 meters above ground was between 3.4% and 9.4%. Conversely, at a upland location experiencing higher wind speeds, the mean undercatch ranged from 11.2% to 23%. The study noted an increase in undercatch for gauges installed at a height of 2 meters. *Pollock et al.* (2018) proposes linear relationships between catch efficiency and wind speed.

Our reference application is the combination of numerical model outputs with in-situ observations to achieve an accurate representation of hourly precipitation across Norway. Directly utilizing hourly in-situ observations leads to an underestimation of precipitation in the merged datasets. Consequently, the adjustment of in-situ observations is needed. In our case, this adjustment addresses only point (a) from the previously mentioned list, which concerns the correction of hourly observations for wind-induced precipitation loss. The primary aim of this document is not to devise a correction method, but rather to examine the effect of applying such corrections on the in-situ observations used in the process of combining them with numerical model output.

For our analysis in Norway, we reference the correction methodologies outlined in two key studies: *Førland et al.* (1996) and *Wolff et al.* (2015). The work by *Førland et al.* (1996) serves as a guide for correcting Nordic precipitation data, introducing both a Dynamic Correction Model (DCM) and a Simple Correction Model (SCM). The DCM, applicable when temperature and wind speed data are available, was utilized by *Michelson* (2004) to correct 12-hour precipitation observations in Sweden, leveraging wind speed and temperature from reanalysis data, a methodology closely aligned with our planned approach. Conversely, the SCM, suitable for situations lacking wind speed data, employs correction factors based on the exposure classification of the station's location. We regard *Wolff et al.* (2015) as an advancement of the methods introduced by *Førland et al.* (1996), specifically for solid precipitation. Our approach aims to integrate these two methodologies: *Wolff et al.* (2015) method for solid precipitation and *Førland et al.* (1996) for liquid precipitation, with a significant modification: instead of relying on measurements from the precipitation observation sites, we utilize meteorological data derived from numerical model outputs for correcting observed precipitation.

This methodological choice significantly changes the purpose of the correction. While the metrological study by *Wolff et al.* (2015) aimed to refine the accuracy and precision of precipitation estimates at a specific location, our goal is still to adjust precipitation data towards the (unknown) true values but we intend to implement this correction across our entire domain, independent of the availability of weather stations. Consequently, our expectations on the quality of our corrections are more modest compared to those in a metrological study. A compromise inherent in our approach is the incorporation of errors from the numerical model into our corrections, a necessary concession to achieve widespread application of the precipitation correction. We intend to apply precipitation

corrections across the study domain, emphasizing areas where atmospheric conditions suggest a higher likelihood of significant observational precipitation loss. Thus, the adjusted observations should, on average, more accurately reflect the actual precipitation patterns, albeit they may still exhibit systematic biases.

To evaluate corrections across the entire domain, we require reference values for true precipitation over this area. Unfortunately, such observed reference values are scarce, available at only a very limited number of locations. For example, the study conducted by *Wolff et al.* (2015) utilized data from a single site, Haukeliseter in Norway, selected for its frequent snow events and high wind speeds during its lengthy winters of 6 to 7 months. In our study, we have chosen to use the annual precipitation climatology derived from numerical model outputs as our reference. We acknowledge the inherent uncertainties in precipitation data reconstructed by numerical models. Typically, the accuracy of model-simulated precipitation fields is assessed using in-situ observations, essentially the reverse of the approach we intend to adopt. However, numerical models generate precipitation estimates through a set of equations, meaning their errors are independent of those associated with measurement techniques. Moreover, the uncertainty related to precipitation fields predicted by numerical models, including reanalyses, has been decreasing over the last decade (*Simmons et al.*, 2017), particularly in Europe (*Bandhauer et al.*, 2022; *Lavers et al.*, 2022). Consequently, we assume that an aggregated climatological value of precipitation from a numerical model, which has demonstrated reasonable accuracy at a local scale, could serve as an adequate proxy for the true, albeit unknown, precipitation values.

The document is structured as follows: Section 2 provides an overview of the in-situ observations and the numerical model utilized in our study. Section 3 details the methodologies employed for precipitation correction and their integration. Section 4 reports the findings from our experiments. These findings are subsequently synthesized in the Conclusions section.

# 2 Data

## 2.1 In-situ Observation

We utilized hourly precipitation observations collected by automatic weather stations operated by MET Norway. These data were accessed through the climate database via the *frost.met.no* API, ensuring that the hourly observations underwent MET Norway's standard quality assurance protocols. Our selection criteria included only those stations equipped with heated rain gauges, thereby enhancing measurement accuracy under cold temperature conditions. The study period spans from September 2019 to September 2023, with a total of 128 rain gauges identified from the metadata database. Corrections were applied to the hourly data, while the validation process focused on annual precipitation totals, resulting in four annual total precipitation values per station. A station yearly time series was excluded if the available data accounted for less than 80% of the total annual

hours. Stations that had fewer than three out of four yearly time series available were also excluded from the study. Consequently, the final number of stations included in our study is 74.

### 2.2 NORA3 and MET Nordic Long-Term Consistent

The Norwegian reanalysis NORA3 (*Haakenstad et al.*, 2021) is provided on a regular grid with spacing of 3 km spanning from 1970 to the present. This dataset results from dynamically downscaling the ERA5 reanalysis (*Hersbach et al.*, 2020). NORA3 employs a convection-permitting, non-hydrostatic numerical weather prediction model to reconstruct the atmospheric state over northern Europe, focusing on Norway. The research presented by *Haakenstad and Øyvind Breivik* (2022) shows that NORA3 better represents precipitation compared to both ERA5 and the earlier hydrostatic 10 km Norwegian Hindcast Archive (NORA10, *Reistad et al.*, 2011).

NORA3 precipitation data have been further refined to a 1 km grid in MET Nordic Long-Term Consistent (LTC) dataset, which is the dataset used in this study.

## 3 Methods

The general form of the adjustment function we will consider approximates Eq. (6.1) reported in the guide *WMO-No.8* (2021). Specifically, our focus will be on the effects of wind field deformation, represented by the equation:

$$\mathrm{P}_k = k \cdot \mathrm{P}_g \tag{1}$$

where: $\mathrm{P}_k$ is the adjusted precipitation amount; $\mathrm{P}_g$ is the measured amount of precipitation in the gauge; $k$ is the adjustment factor for the effects of wind field deformation. $k$ is the reciprocal of the catch ratio $R$.

It is important to note that the equations for computing the correction factor vary between liquid (rain) and solid (snow) forms of precipitation. Regarding notation, we will follow the conventions established by the CIMO Guide *WMO-No.8* (2021), using the subscripts $r$ and $s$ to denote quantities related to liquid and solid precipitation, respectively (e.g., $k_s$ will represent the correction factor for solid precipitation).

### 3.1 Solid Precipitation

The continuous adjustment function proposed by *Wolff et al.* (2015) for correcting wind-induced loss of solid precipitation operates by adjusting the observed precipitation. The corrected precipitation is derived by multiplying the observed amount by the inverse of the catch ratio $R$ defined as (see Equation (10) of *Wolff et al.* (2015)):

$$R = [1 - \tau_1 - (\tau_2 - \tau_1)\mathrm{f}(\mathrm{T}; \mathrm{T}_\tau, \mathrm{s}_\tau)] \exp\left[-\left(\frac{V}{\theta}\right)^{\beta}\right] + \tau_1 + (\tau_2 - \tau_1)\mathrm{f}(\mathrm{T}; \mathrm{T}_\tau, \mathrm{s}_\tau) \tag{2}$$

where: $T$ represents temperature and $V$ denotes wind speed. The function $\mathrm{f(T;T_\tau,s_\tau)}$ introduces temperature dependence:

$$\mathrm{f(T;T_\tau,s_\tau)} = \frac{\exp\left[(T-T_\tau)/s_\tau\right]}{1+\exp\left[(T-T_\tau)/s_\tau\right]} \tag{3}$$

Note that Equation (11) in *Wolff et al.* (2015) presents a formulation for temperature-dependent regression noise, $\sigma(T)$, which could potentially inform the uncertainty associated with precipitation correction. Upon implementation, we observed that this often resulted in significantly high values of $k$. *Wolff et al.* (2015) in their Section 5.3, discuss the implications of regression noise and uncertainty analysis, highlighting that Equation (11) does not optimally characterize regression noise. Consequently, we have decided not to incorporate this aspect into our study.

After the optimization of the parameters of Eq. (2), *Wolff et al.* (2015) derived their Equations (12) and (13), depending on whether the wind speed is considered at 10 meters above the ground or at the gauge height, respectively. We will refer to **Correction A** when the correction is applied with the 10m wind speed as input and to **Correction B** when the correction is applied with the wind speed at the gauge height. For both corrections, the parameter values are reported in Table 1 of *Wolff et al.* (2015), which is replicated here as Tab. 1.

Numerical models typically provide wind speed measurements at 10 meters above the ground. To adjust the wind speed to gauge height, assumed to be 1.5 meters above the ground, we employ a transformation based on the "log-wind profile" assumption, similar to the approach used by *Michelson* (2004). This transformation assumes a fixed roughness length of 0.25 m:

$$V_g = \left[\ln\left(\frac{1.5\mathrm{m}}{0.25\mathrm{m}}\right)/\ln\left(\frac{10\mathrm{m}}{0.25\mathrm{m}}\right)\right] V_{10m} \tag{4}$$

With our approximation, the correction factor to transform the 10m wind speed to 1.5m wind speed is equal to 0.49.

From the Conclusions of *Wolff et al.* (2015):

> The under-catch has a pronounced relation to temperature and a non-linear relation to wind speed. For solid precipitation at $-2°C$ or below, only 80% of the assumed true precipitation is caught at wind speeds of $2\,\mathrm{m\,s^{-1}}$, and only 40% at $5\,\mathrm{m\,s^{-1}}$. The slope of the catch ratio then levels off markedly and stabilizes at 20% at $7-8\,\mathrm{m\,s^{-1}}$. This base line level is confirmed with data up to $15-20\,\mathrm{m\,s^{-1}}$ and will most likely not change for even higher wind speeds.

Again, from the Conclusions of *Wolff et al.* (2015) but about the limits of applicability of the adjustment:

> The result is one continuous equation which describes the wind-induced under-catch for snow, mixed precipitation and rain events for wind speeds up to at least $20\,\mathrm{m\,s^{-1}}$ and temperatures up to 3 °C. Input parameters are wind speed and air temperature, thus

allowing for easy application at operational weather stations only equipped with basic sensors.

In Figures 1- 5, the correction factors are shown. When the figures indicate a correction factor of e.g. 1.1, this should be interpreted as an overall correction of 10% to the initially measured precipitation.

The SCM described by *Førland et al.* (1996) was adopted in Norway by *Mohr* (2009) to adjust daily precipitation data for the seNorge observational gridded dataset, with correction factors outlined in Tab. 2. Notably, these correction factors allow for a maximum adjustment of +80% in cases of highly exposed sites in coastal and mountain regions, a significantly smaller correction compared to that introduced by the DCM or by *Wolff et al.* (2015). It is important to note that *Førland et al.* (1996) mentions these correction factors were initially created to adjust monthly values for shielded Nordic gauges, with unshielded gauges requiring an adjustement of the correction factors of approximately 5% more for liquid precipitation and 50% more for solid precipitation. Although the corrections on a daily or sub-daily scale may exceed +80%, the SCM correction factors offer an estimate of the difference between raw (i.e. unadjusted) and corrected monthly accumulated precipitation values.

### 3.2 Liquid Precipitation

As highlighted in the Introduction, the research conducted by *Førland et al.* (1996), *Pollock et al.* (2018), and the guidance provided in the WMO guide *WMO-No.8* (2021) reveal that observational data tend to underestimate not just solid precipitation but liquid precipitation as well. However, the correction method proposed by *Wolff et al.* (2015) does not address adjustments for liquid precipitation, largely because it falls outside the scope of this particular correction applicability.

The DCM correction factor for solid precipitation is:

$$k = \exp\left[-0.00101 \cdot \ln(\mathrm{P}_g) - 0.012177 \cdot V_g \cdot \ln(\mathrm{P}_g) + 0.034331 \cdot V_g + 0.007697 - 0.05\right] \quad (5)$$

The DCM incorporates wind speed and precipitation intensity for its corrections of liquid precipitation, whereas the SCM utilizes correction factors, as detailed in Tab. 2. These factors indicate that, on a monthly aggregate basis, the discrepancy between raw and adjusted totals of liquid precipitation varies between 2% and 14%, contingent upon the site exposure. These adjustments for liquid precipitation are notably less extensive than those for solid precipitation, which exhibit corrections ranging from 5% to 80% at the monthly scale.

### 3.3 Combining the adjustments for solid and liquid precipitation

Our objective is to adjust liquid and solid precipitation using a continuous function. Therefore, we need to combine the equations used to compute $k$ for both states of precipitation.

We assume that: for temperatures below 1 °C, $k = k_s$, directly applying the correction for solid precipitation in Eq. (2); for temperatures above 3 °C, $k = k_r$, directly applying the correction for

liquid precipitation Eq. (5); for temperatures within 1 °C to 3 °C, a smooth transition function can be used to calculate $k$, transitioning from $k_s$ to $k_r$. The equation for $k$ can be written as:

$$k = \begin{cases} k_s, & \text{if } T \leq 1\,^{\circ}\text{C} \\ (1-T)^2 / \left[(1-T)^2 + (3-T)^2\right](k_r - k_s), & \text{if } 1\,^{\circ}\text{C} < T < 3\,^{\circ}\text{C} \\ k_r, & \text{if } T \geq 3\,^{\circ}\text{C} \end{cases} \tag{6}$$

In Figures 6- 10, the correction factors obtained using Eq. (6) are shown. As detailed in Section 3.1, we introduce **Correction A** for cases where $k_s$ is calculated using a configuration that inputs the 10m wind speed, and **Correction B** when $k_s$ is derived using a configuration with the wind speed adjusted to gauge height. It is important to note that the 10m wind speed from the numerical model output serves as the wind speed input for both corrections. However, for **Correction A**, this wind speed is used directly, whereas for **Correction B**, the wind speed is scaled down to 1.5m to reflect conditions closer to gauge height. For temperatures lower than 1 °C, $k$ is the same as reported in Figures 1- 5. For temperatures greater than 3 °C, $k$ becomes independent of the temperature but depends only on the precipitation intensity and wind speed.

# 4 Results

We analyze 74 time series of hourly precipitation amounts from in-situ observations, as outlined in Sec. 2.1. Concurrently, we retrieve hourly precipitation data from numerical model outputs for identical locations and their surroundings. These data are subsequently aggregated over a 1-year period, choosing September of one year to September of the following year to represent the hydrological year in the annual totals. We consider the 4 hydrological years from 2019 to 2023, specifically: 2019–2020, 2020–2021, 2021–2022 and 2022–2023.

In terms of mathematical notation, hourly precipitation is denoted by $P$. As described in Sec. 3, the subscripts serve specific purposes: $k$ represents corrected precipitation, $g$ signifies raw observed precipitation, and $m$ denotes precipitation derived from model fields. For corrected precipitation, superscripts A and B are utilized to differentiate between the two correction methods outlined in Sec. 3.3. The annual totals are denoted by $A$, with $A_m$ indicating the total annual precipitation derived from model data at a specific location. The deviation between observed (either raw or corrected) and modeled annual totals is represented by $D$. Specifically, the differences are calculated as follows: $D_g = A_g - A_m$ for raw observed precipitation, $D_k^{\mathrm{A}} = A_k^{\mathrm{A}} - A_m$ for precipitation corrected using method A, and $D_k^{\mathrm{B}} = A_k^{\mathrm{B}} - A_m$ for precipitation corrected using method B. The mean annual total precipitation over the four hydrological years is symbolized by $\overline{A}$, accompanied by the appropriate subscript to indicate the specific data type being referred to. Analogously, $\overline{D}$ indicates a mean annual deviation.

The correction of hourly precipitation for the hydrological year 2022–2023 is illustrated at three locations: Oslo, Bergen, and Tromsø, shown in Figs. 11, 12, and 13, respectively. These figures

aim to provide insights into the process of the corrections throughout an entire hydrological year.

A comprehensive analysis of the impact of these corrections across 74 stations is detailed in Tables 3 to 5. For each station, the annual total predicted by the model, denoted as $\overline{A_m}$, serves as a reference point. The average deviations based on raw precipitation data are represented by $\overline{D_g}$, both as absolute figures in millimeters and as relative deviations in percentages ($\overline{D_g}/\overline{A_m} \times 100$). These raw precipitation values establish a baseline for assessing the effects of the corrections, which are quantified in the tables as $\overline{D_k^{\mathrm{A}}}$ and $\overline{D_k^{\mathrm{B}}}$, along with their respective relative deviations ($\overline{D_k^{\mathrm{A}}}/\overline{A_m} \times 100$ and $\overline{D_k^{\mathrm{B}}}/\overline{A_m} \times 100$).

Figures 14, 15, and 16 visually summarize the relative deviations mentioned in parentheses in the aforementioned Tables 3 to 5. The annual total precipitation reported by raw observations is on average 10% less than the modelled value. Upon applying the corrections, there is an increase in precipitation amounts, as depicted in Figs. 15 to 16. Corrected observations more closely match model predictions with Correction B, whereas Correction A tends to yield higher values than those modeled. Specifically, Fig. 16 shows that precipitation corrected with Correction B has a median relative deviation of -4%, with half of the stations displaying deviations between -15% and 9%. While corrections enhance the congruence between observed data and model predictions on average, they also expand the spread of relative deviation distributions. For raw measurements, deviations range from -52% to 23%, with an interquartile range of -21% to 1%. Correction B, however, extends this range to -50% to 53%, with an interquartile range of -15% to 9%. Notably, the broader range, especially in the upper deviations, presents challenges for validation using our current method, which is primarily designed for evaluating mean regional values.

The larger relative deviations in corrected annual precipitation totals could be a consequence of uncertainties in the modeled 10m wind speed predictions. Systematic overestimations of modeled wind speeds, relative to observed values, could lead to inaccurately high corrected precipitation totals. In Figures 17 and 18, we examine the comparison between modeled and observed hourly 10m wind speeds at station locations, presenting the correlation and bias, respectively. The correlation between modeled and observed wind speeds is generally good, with a median value of 0.68 and a relatively narrow interquartile range. Up to this point, the 10m wind speed from the model is determined at station locations using a nearest neighbor approach. To enhance the temporal stability of the modeled wind and mitigate the effects of minor inaccuracies in the placement of weather phenomena within the model, we propose averaging the values from several grid points closest to the station locations. Our preliminary analysis indicates that the correlation between modeled and observed wind speeds remains largely unchanged when using aggregated values from up to the nearest 200 grid points. However, the bias shifts significantly, as illustrated in Figures 19 and 20. Specifically, the average modeled value, when aggregated, tends to be higher than that obtained via the nearest neighbor method, with the degree of overestimation increasing alongside the number of grid points considered in the aggregation.

To mitigate the impact of model prediction uncertainties on corrected precipitation —partic-

ularly the high values in the right tail of the distribution seen in Fig. 16 which pose validation challenges— we propose two adjustments for refining Correction B: (a) utilizing wind speed derived from aggregated values, and (b) imposing an upper limit on the correction factor $k$ in Eq. 6. In Fig.21, we re-evaluate the results of Fig.16 under these adjustments. Here, the 10m wind speed is calculated as the average of the four nearest grid points to each station, and the correction factor is capped at 2, aligning closely with the maximum correction factor of 1.80 permitted in the SCM.

The outcomes in Fig.21 do not diverge significantly from those in Fig.16. Although the proposed adjustments do not enhance the results, they also do not degrade the performance of Correction B. Therefore, adopting these measures to increase the robustness of the correction against model uncertainty could still be considered a viable strategy.

# 5 Conclusions

The comparison between observed and modeled mean annual total precipitation reveals that observations generally underestimate the modeled precipitation by about 10% of the modeled mean annual total. For half of the stations analyzed, relative deviations ranged from -21% to +1%, as illustrated in Fig.14 and documented in Tables 3 to 5. These findings align with WMO indications *WMO-No.8* (2021) on the uncertainty of precipitation measurements. Furthermore, they align also with the expectations set by SCM correction factors, detailed in Table 2, indicating that stations with siting exposures rated between 1 and 3 should exhibit an average precipitation underestimation of -20% to -2%, varying by precipitation phase.

After implementing the corrections (Sec. 3.3), precipitation totals increase, as illustrated in Figs.15 through 16. Correction B aligns corrected observations more accurately with model forecasts, while Correction A often results in higher precipitation amounts compared to the model. Fig.16 shows that Correction B adjusts precipitation to a median relative deviation of -4%, with deviations ranging from -15% to 9% for half of the stations.

Applying corrections with model data as input, as proposed in Sec.3.3, introduces the possibility of embedding model uncertainties and systematic errors into the corrected data. One observable effect is the increase of the spread of the distribution in Fig.16 compared to Fig. 14, possibly due to a systematic overestimation of the modelled wind at some locations, leading to an overestimation of precipitation in these areas. To mitigate the influence of model uncertainties on the correction, we could consider imposing upper limits on correction factors to prevent model errors from producing unrealistically high precipitation values.

Modifying the approach to derive 10m wind speed from model fields —specifically, by calculating the average wind speed from multiple nearby grid points instead of solely the nearest one— and setting a maximum threshold for the correction factor could lead to a more stable correction process, making it less sensitive to the uncertainties inherent in model data. Nevertheless, this adjustment seems to have a minimal impact on the outcomes, as evidenced by the comparison

between Fig.16 and Fig.16.

Ultimately, we hope that correcting precipitation data will enhance the outcomes of using the combined precipitation fields as input for snow and hydrological modeling, leading to improved model performance and reliability. In this context, an indirect method of validating the corrected precipitation fields involves assessing the performance of snow and hydrological models when these adjusted fields are used as inputs.

# 6 Figures

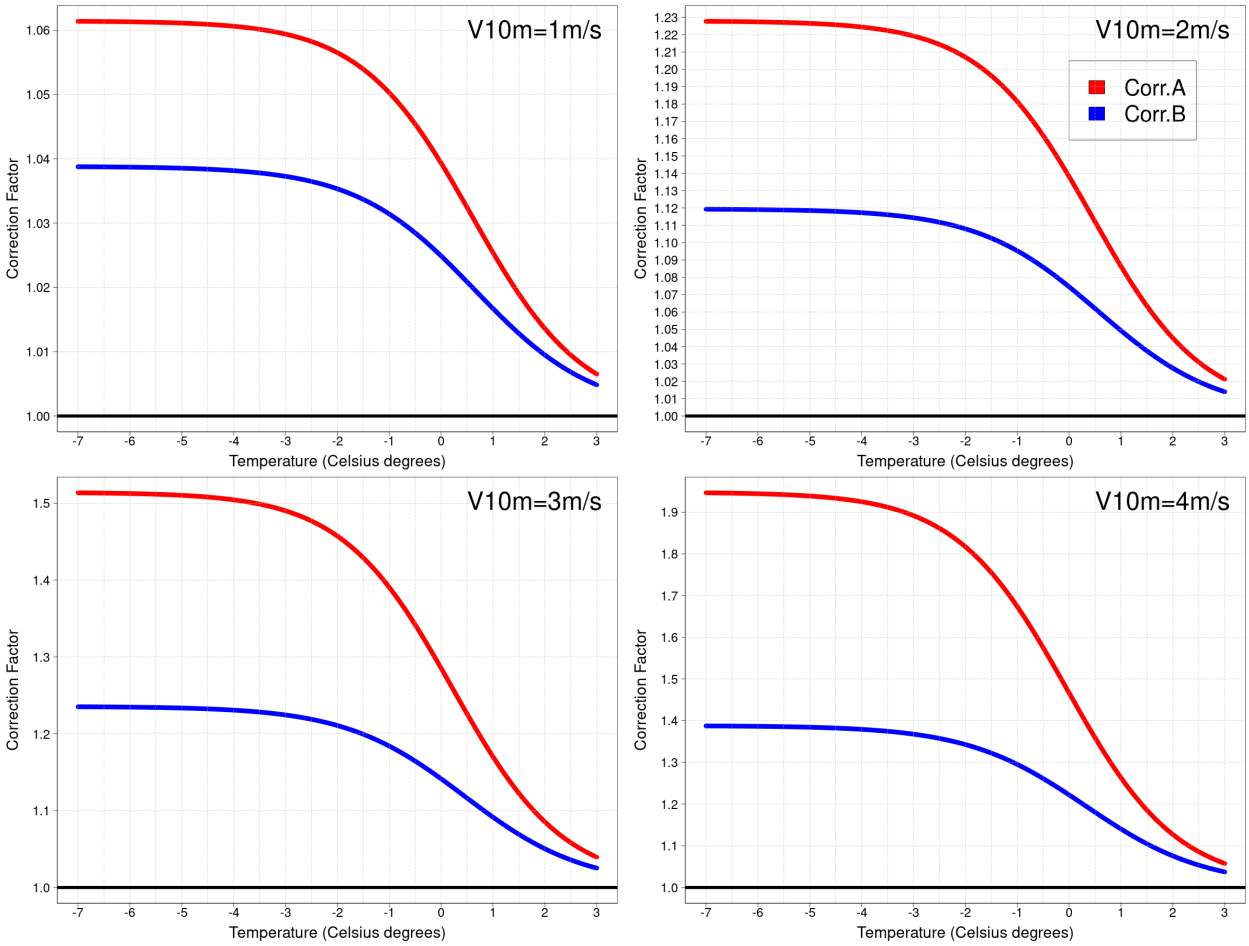


Figure 1: Correction factors as a function of temperature for given 10m wind speeds, based on Eq. 2. The red lines represent **Correction A** using direct 10m wind speed. The blue lines illustrate **Correction B** with 10m wind speed adjusted to 1.5m, typical gauge height.

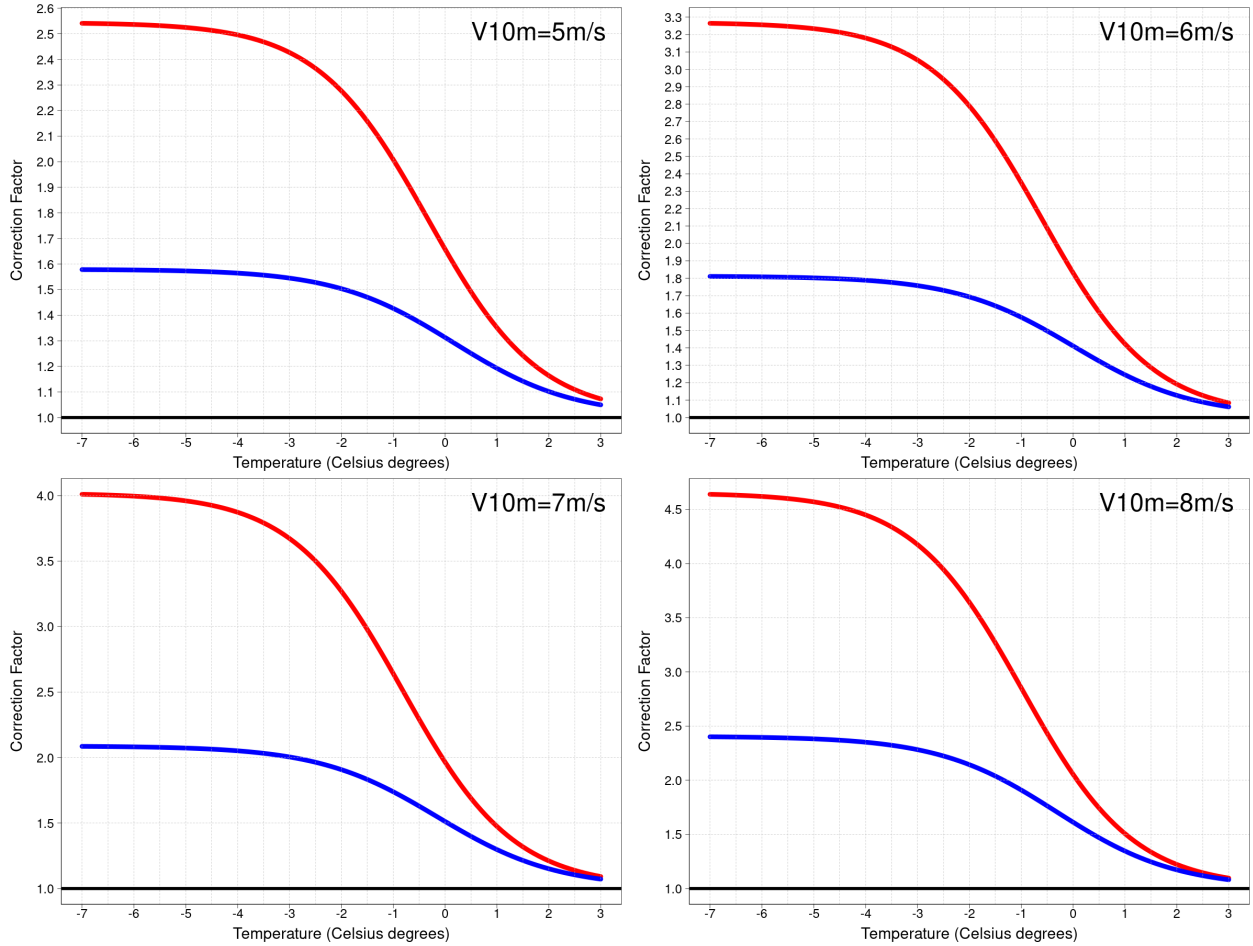


Figure 2: Correction factors as a function of temperature for given 10m wind speeds, based on Eq. 2. The layout is similar to Fig. 1.

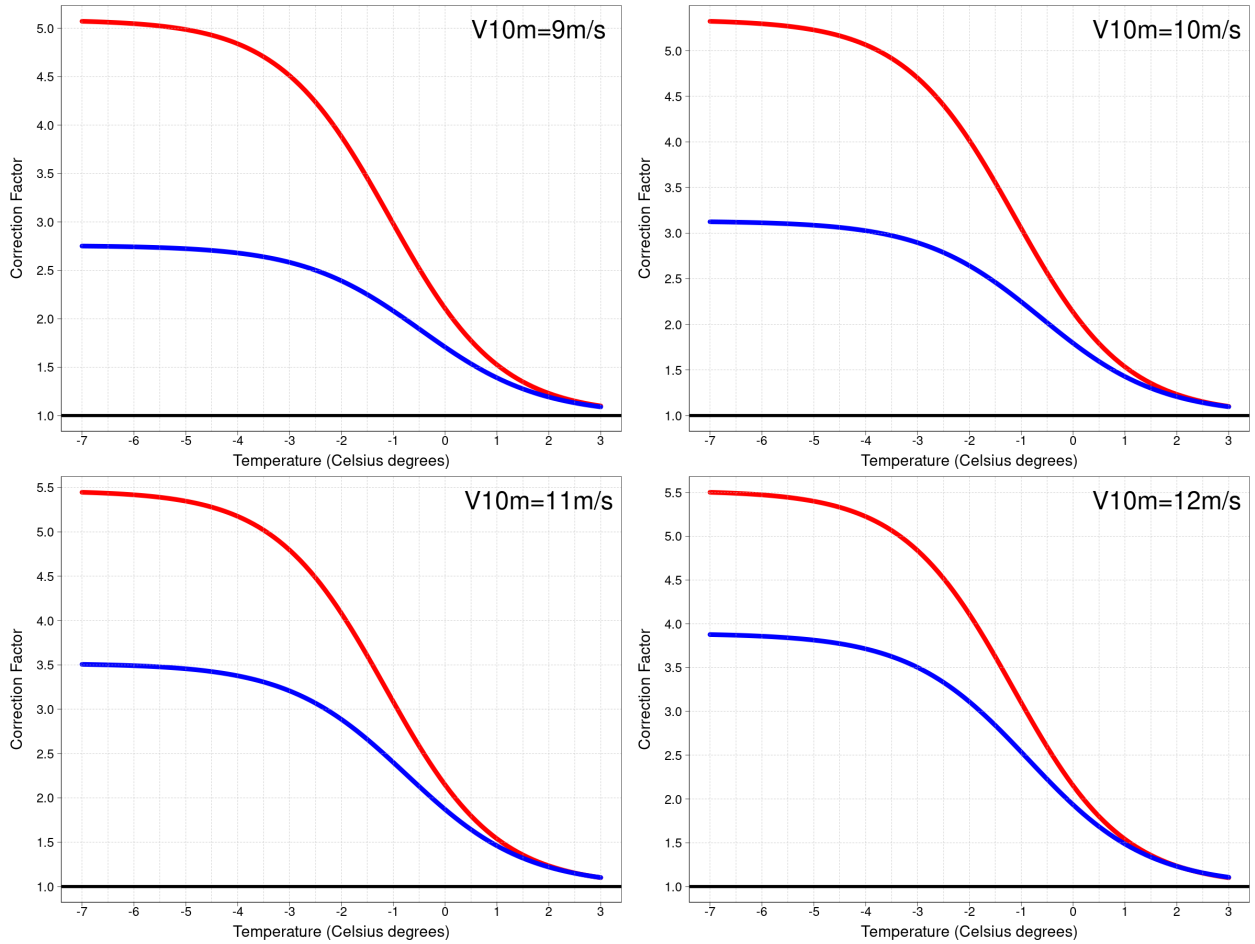


Figure 3: Correction factors as a function of temperature for given 10m wind speeds, based on Eq. 2. The layout is similar to Fig. 1.

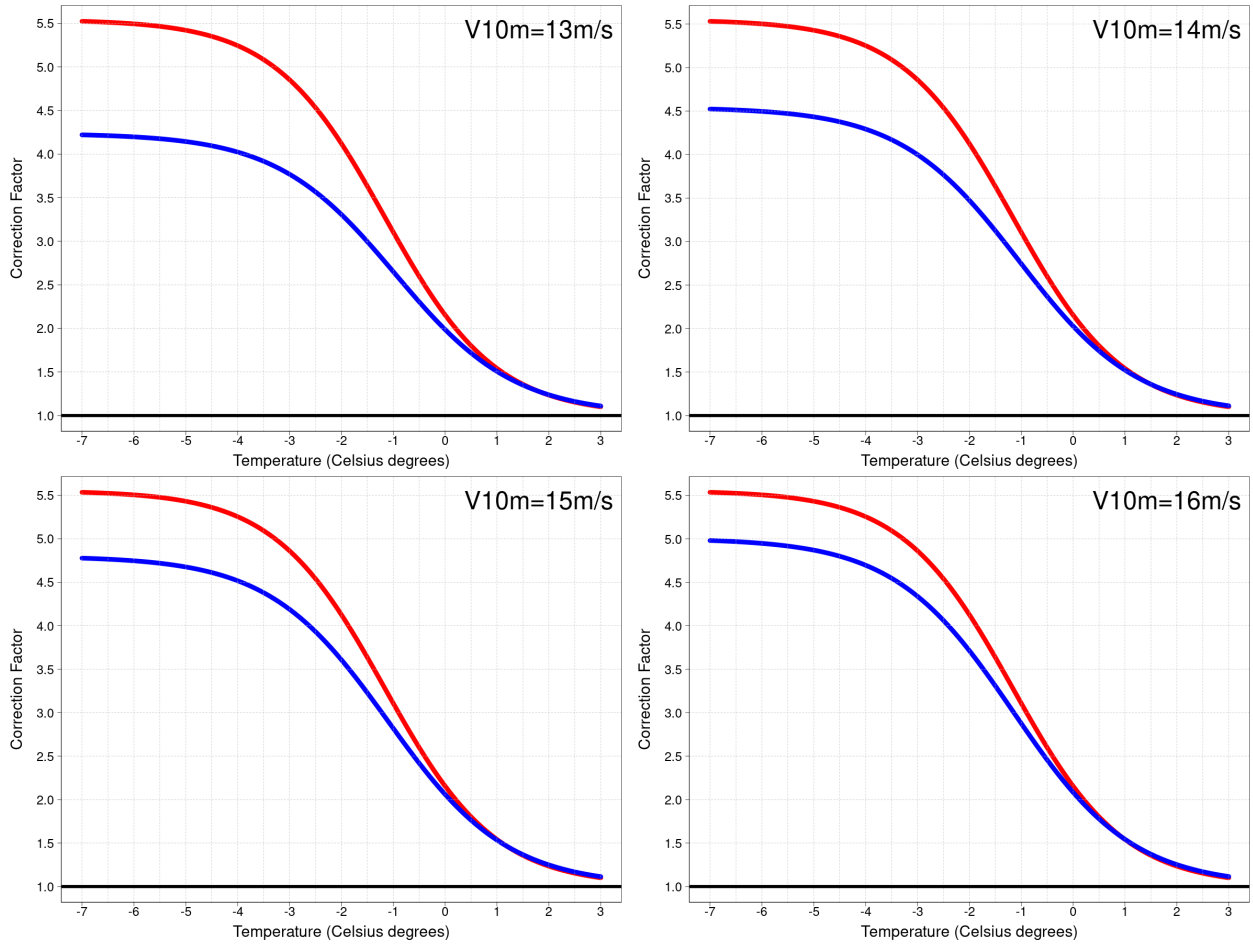


Figure 4: Correction factors as a function of temperature for given 10m wind speeds, based on Eq. 2. The layout is similar to Fig. 1.

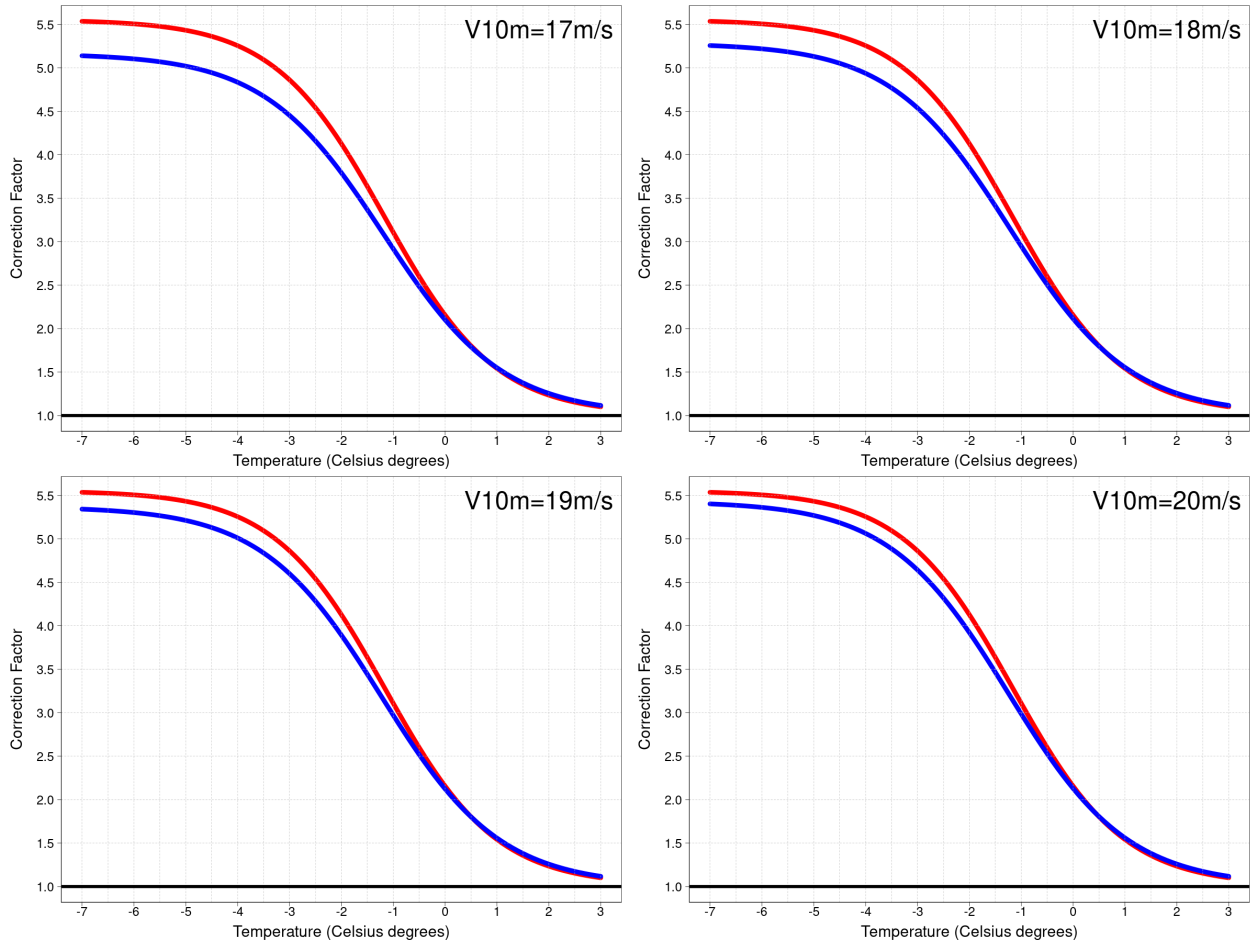


Figure 5: Correction factors as a function of temperature for given 10m wind speeds, based on Eq. 2. The layout is similar to Fig. 1.

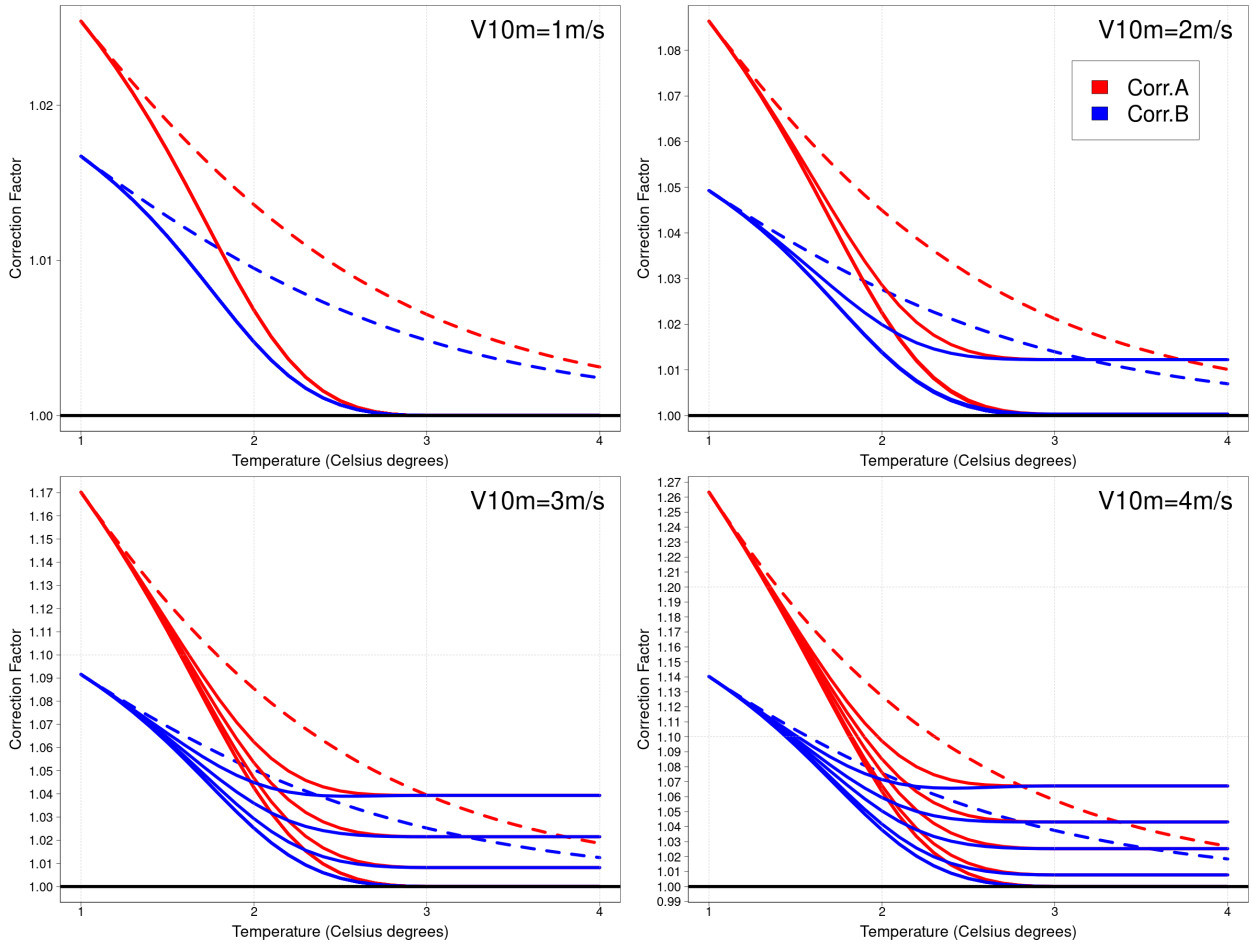


Figure 6: Correction factors as a function of temperature for given 10m wind speeds, based on Eq. (6). The dashed lines show $k$ obtained using Eq. (2). The layout is similar to Fig. 1.

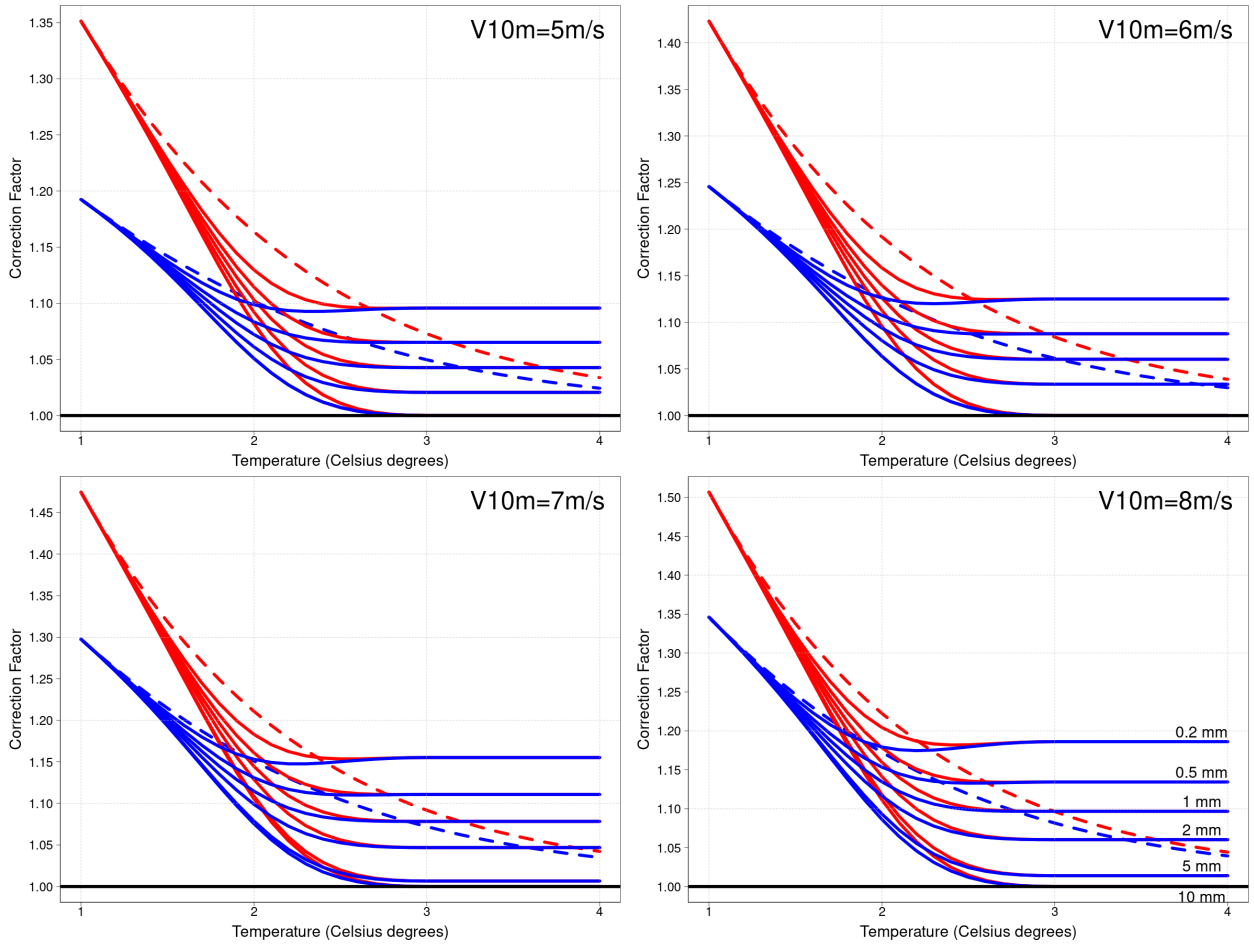


Figure 7: Correction factors as a function of temperature for given 10m wind speeds, based on Eq. (6). The layout is similar to Fig. 6.

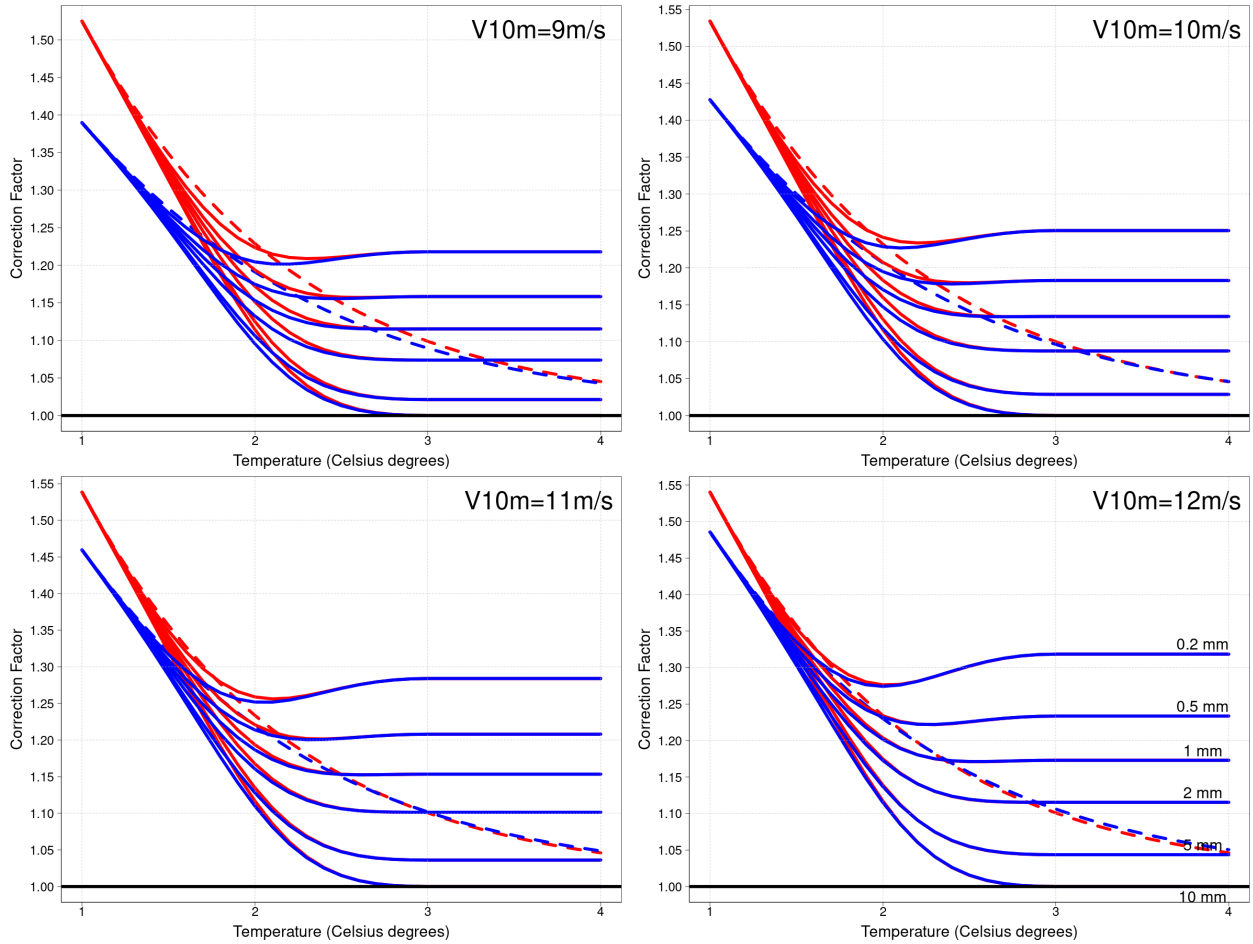


Figure 8: Correction factors as a function of temperature for given 10m wind speeds, based on Eq. (6). The layout is similar to Fig. 6.

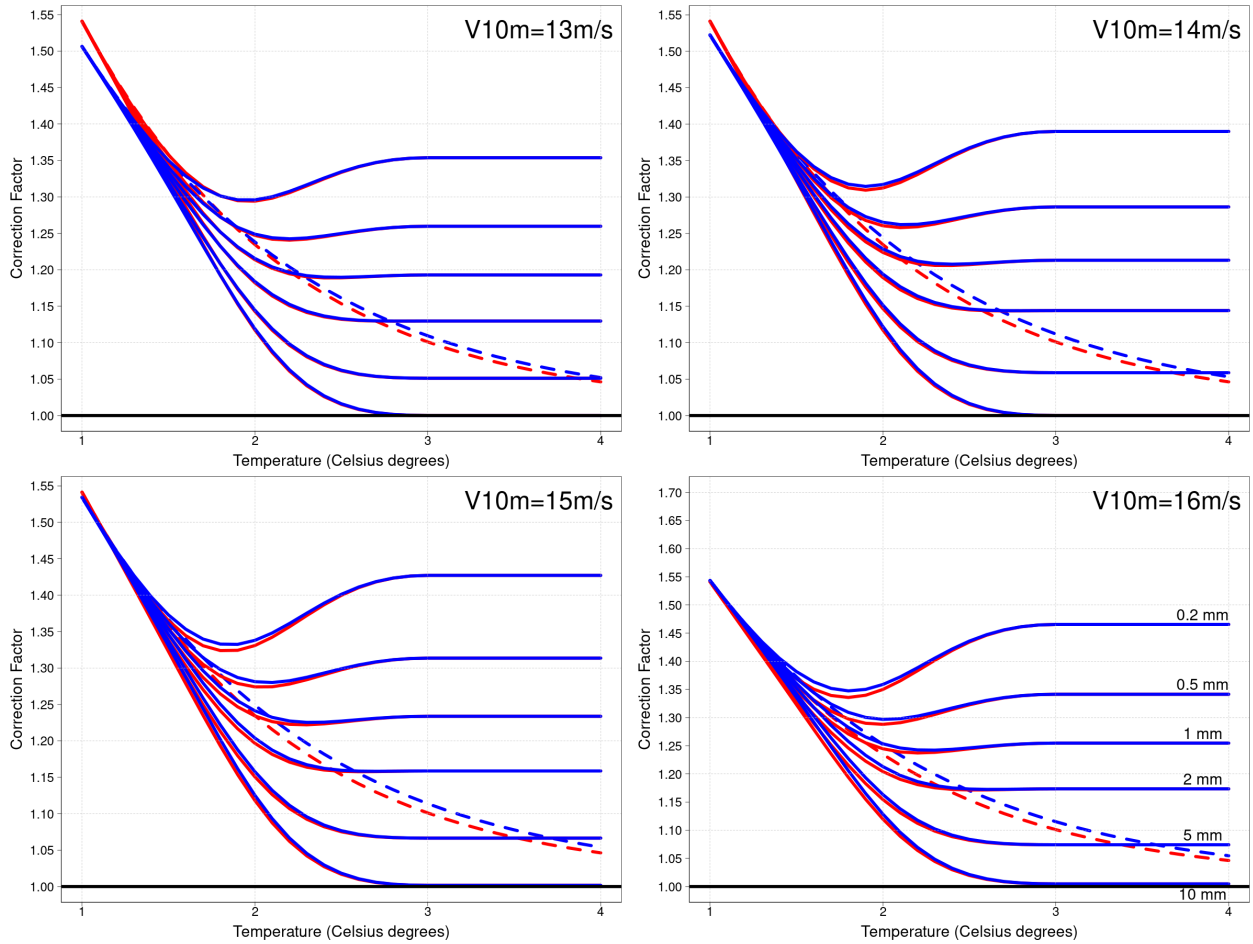


Figure 9: Correction factors as a function of temperature for given 10m wind speeds, based on Eq. (6). The layout is similar to Fig. 6.

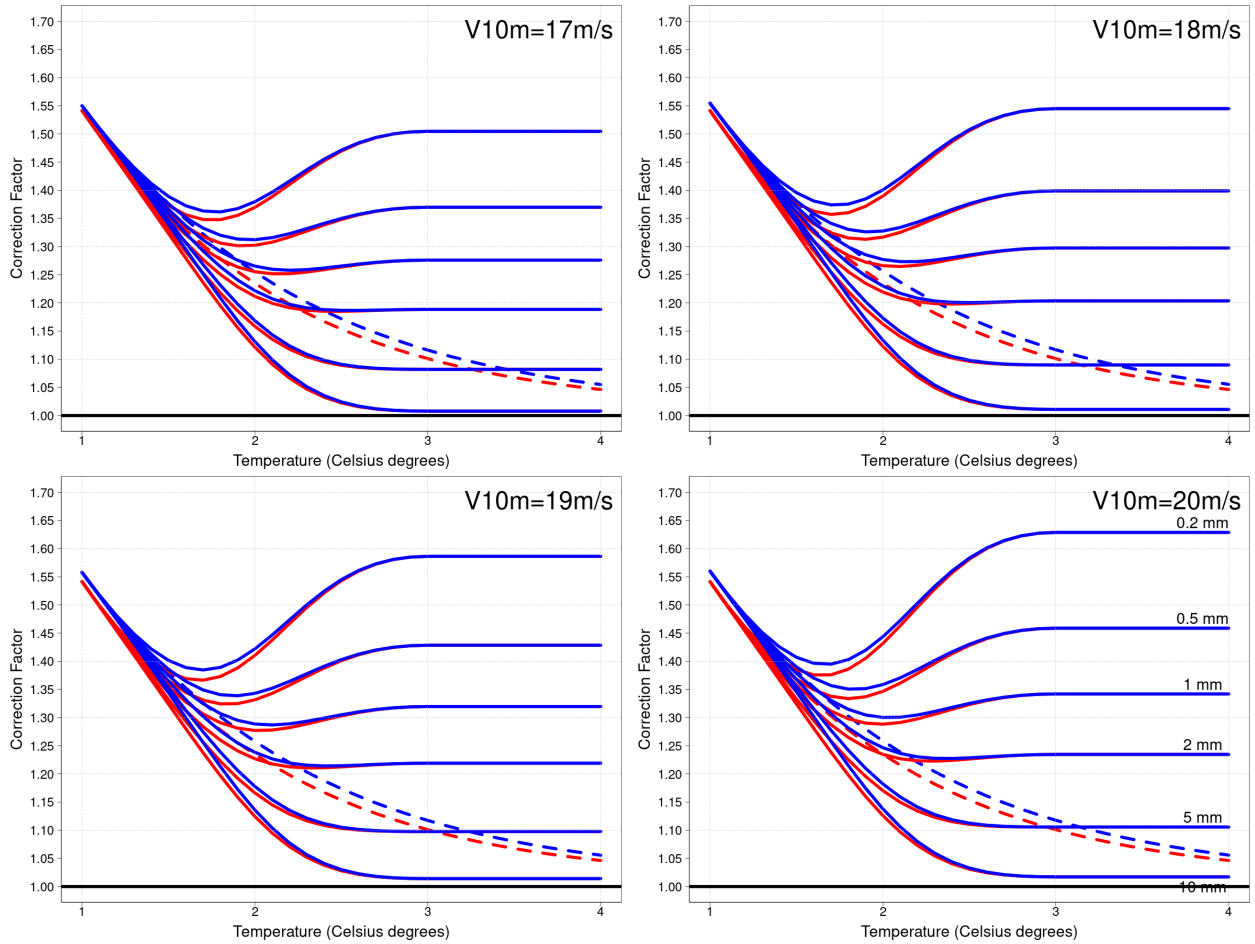


Figure 10: Correction factors as a function of temperature for given 10m wind speeds, based on Eq. (6). The layout is similar to Fig. 6.

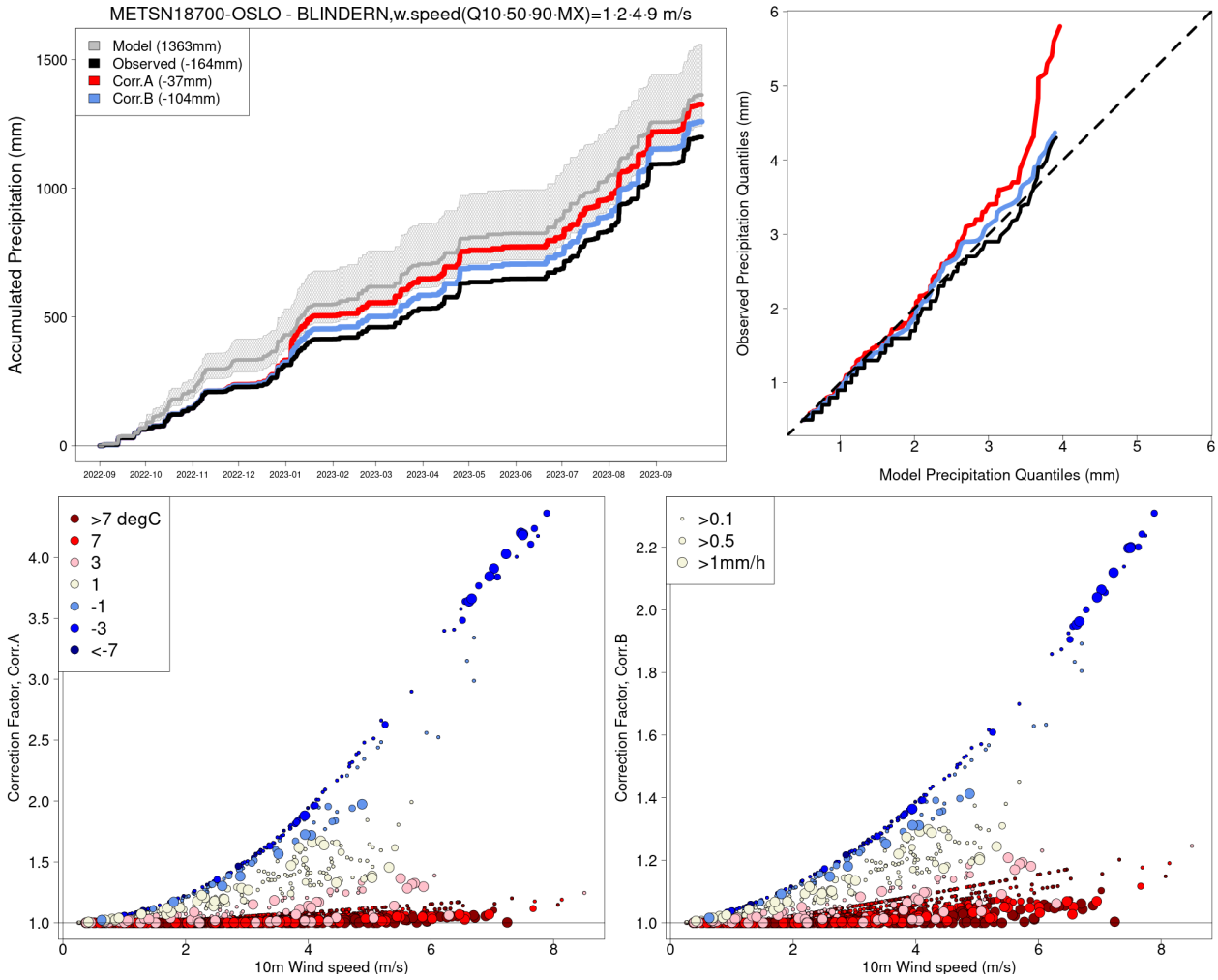


Figure 11: Correction of hourly precipitation for Oslo (Station Identifier=18700) from September 2022 to September 2023, utilizing the methodology outlined in Sec.3.3. The top-left panel presents the time series of accumulated precipitation, with color definitions provided in the legend and the model prediction for the nearest 25 grid points highlighted in gray. The top-right panel displays the quantile-quantile plot for hourly precipitation exceeding 0.5 mm/h. The lower panels illustrate the variation of the correction factor $k$, as defined in Eq.(6), in relation to wind speed and temperature for Corrections A and B (left and right panels, respectively), as specified along the y-axis. Refer to Fig. 6 for additional context.

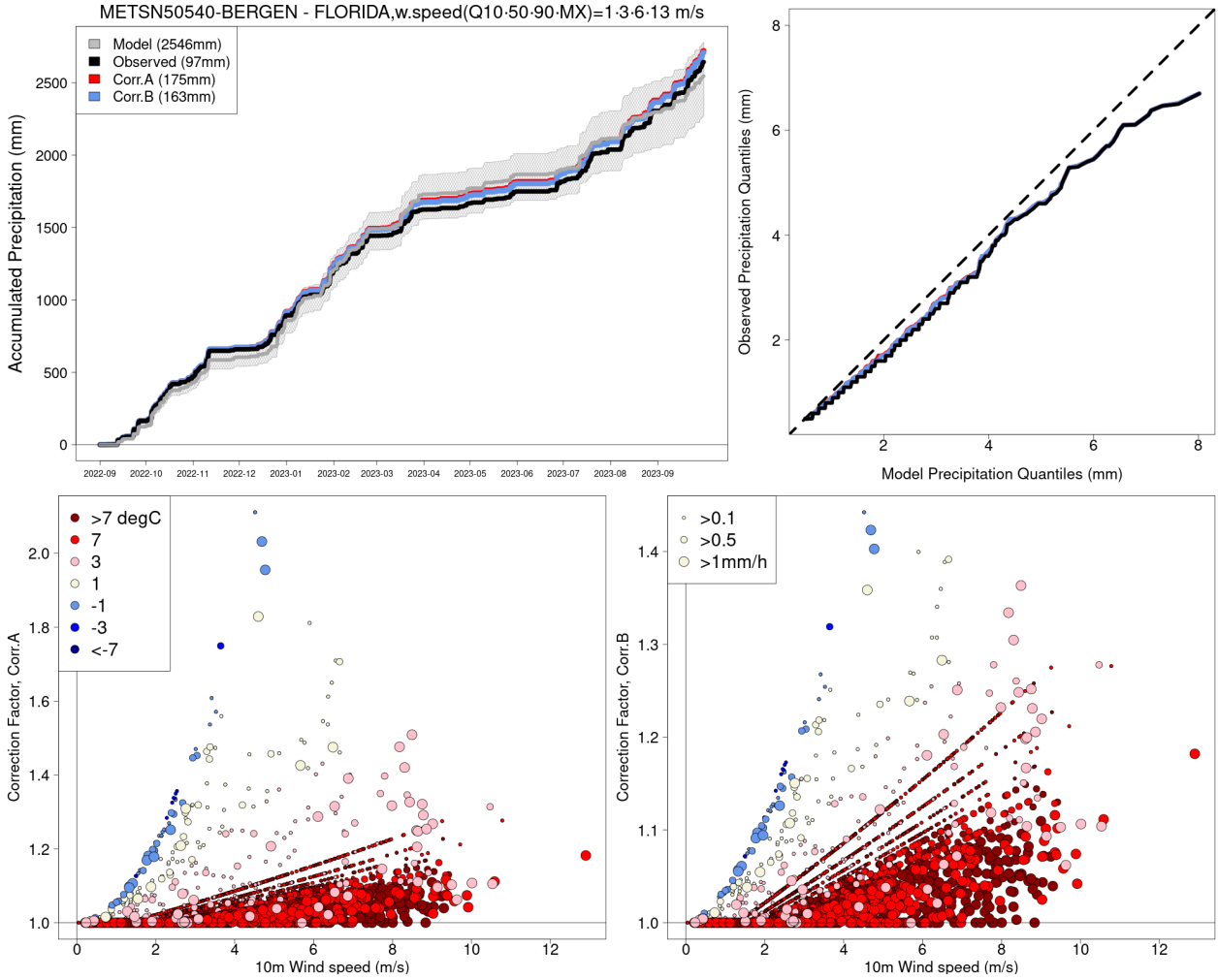


Figure 12: Correction of hourly precipitation for Bergen (Station Identifier=50540) from September 2022 to September 2023, utilizing the methodology outlined in Sec.3.3. The layout is the same as Fig. 11.

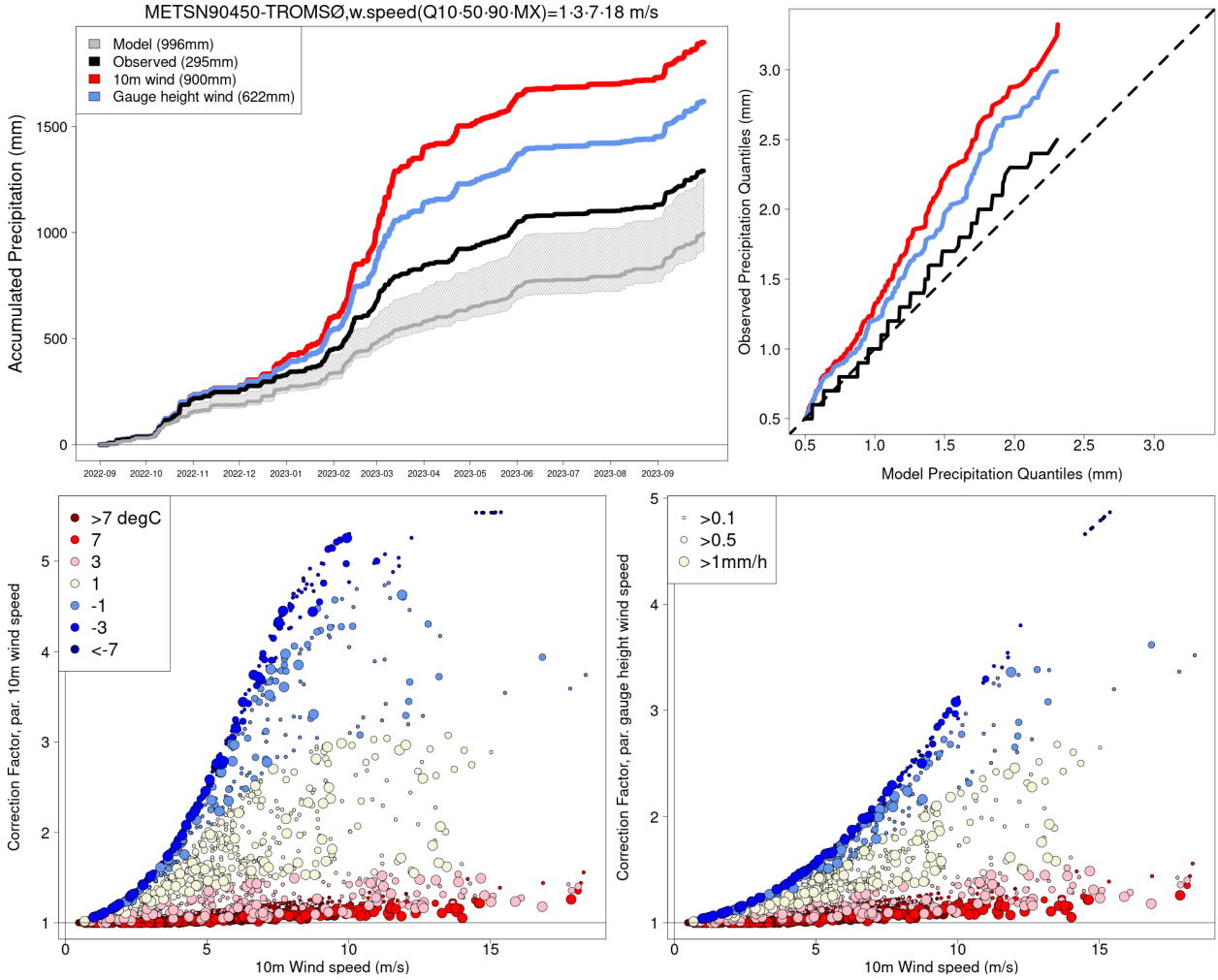


Figure 13: Correction of hourly precipitation for Tromsø (Station Identifier=90450) from September 2022 to September 2023, utilizing the methodology outlined in Sec.3.3. The layout is the same as Fig. 11.

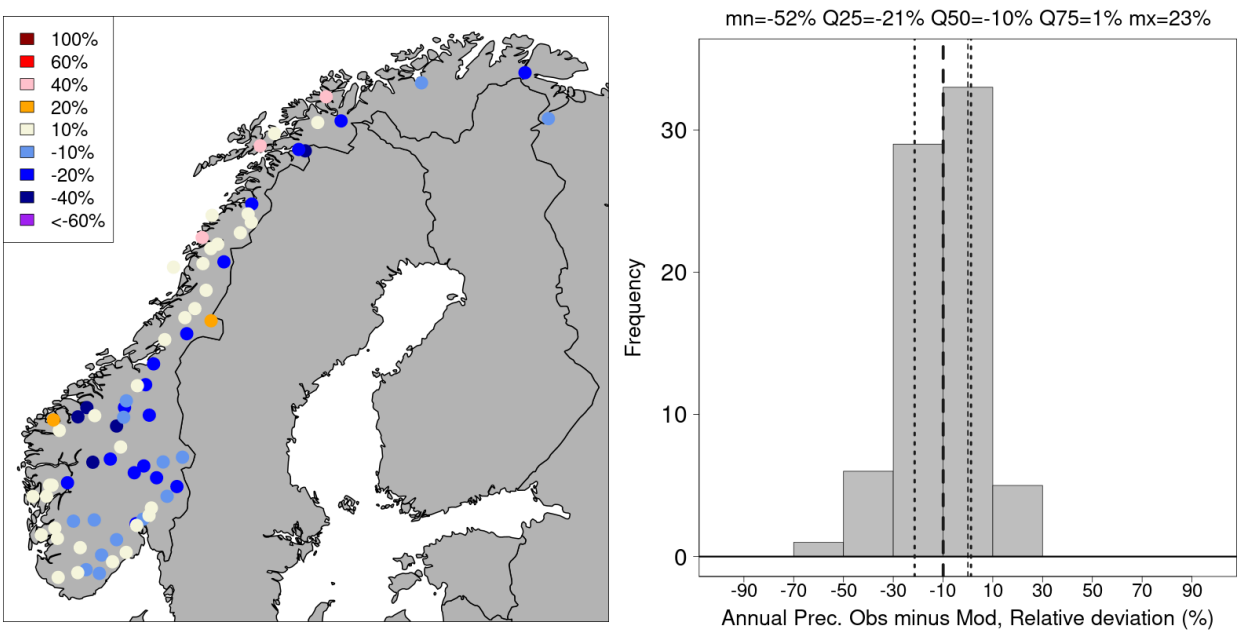


Figure 14: Comparison of observed versus model-predicted mean annual total precipitation for the years 2019–2023 across 74 stations, focusing on the relative deviation $D_g/A_m$ (where, for example, +10% signifies that the observed deviation from the model prediction constitutes 10% of the model mean annual total). The left panel shows the map of the relative deviations, while the right panel displays a histogram of the deviations. In the histogram, thick vertical lines denote the median, 25th, and 75th percentiles, and a lighter vertical line marks the 0% position, indicating no deviation.

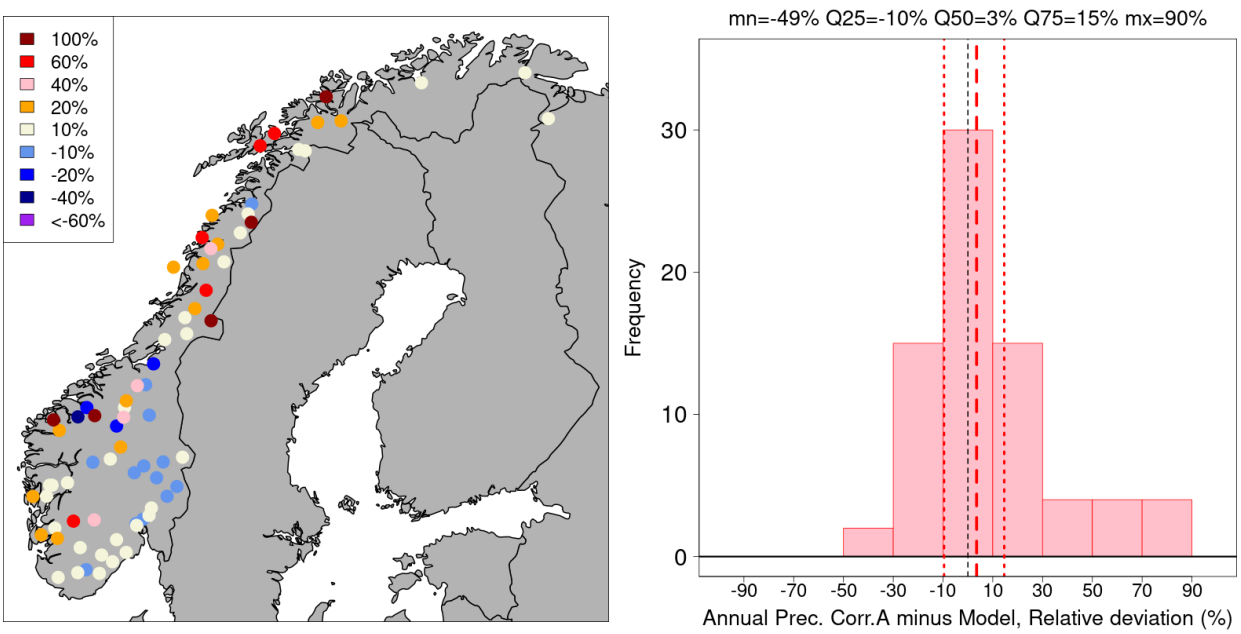


Figure 15: Comparison of corrected (using Correction A) and model-predicted mean annual total precipitation for the period 2019–2023 across 74 stations, with a focus on the relative deviation $D_k^{\mathrm{A}}/A_m$. The layout is similar to Fig. 14.

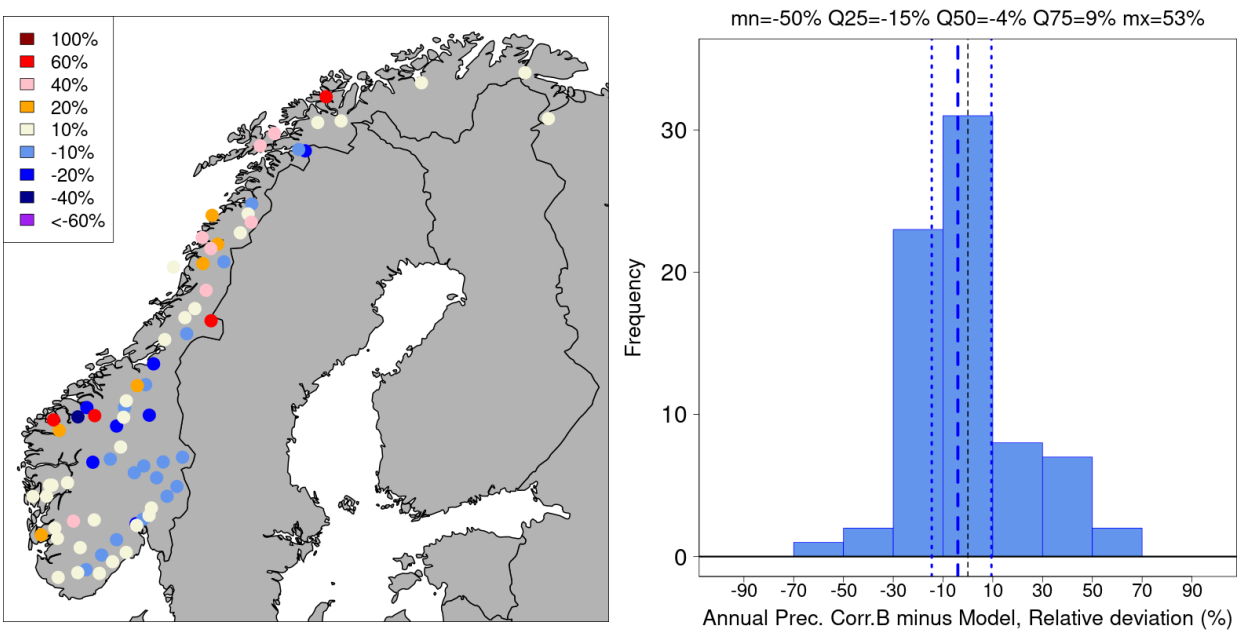


Figure 16: Comparison of corrected (using Correction B) and model-predicted mean annual total precipitation for the period 2019–2023 across 74 stations, with a focus on the relative deviation $D_k^{\mathrm{B}}/A_m$. The layout is similar to Fig. 14.

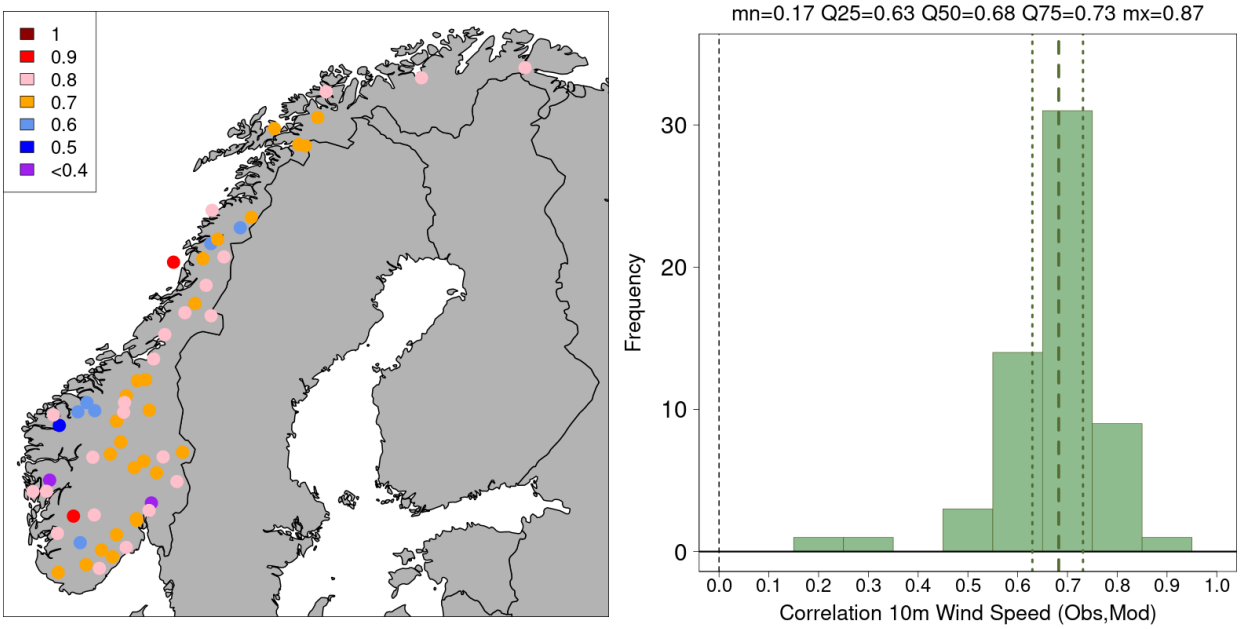


Figure 17: Pearson's correlation coefficient of 10m hourly wind speed between modeled and observed data for the period 2019–2023 across 74 stations.

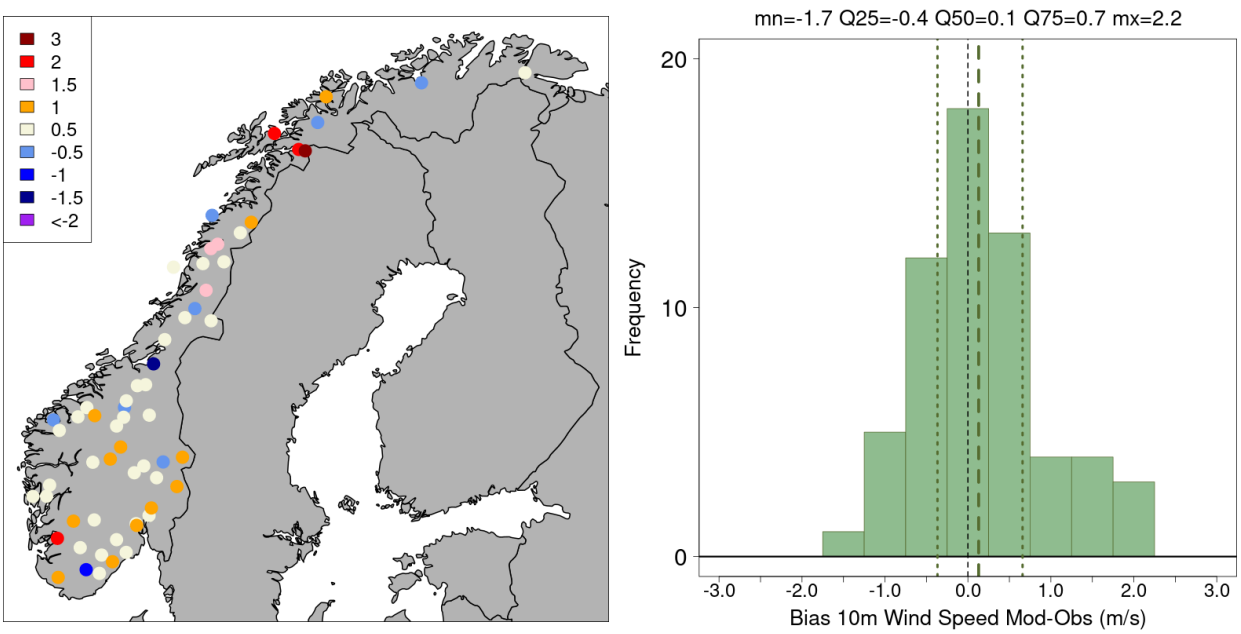


Figure 18: Mean error (or bias) of 10m hourly wind speed between modeled and observed data (Model minus Observations) for the period 2019–2023 across 74 stations.

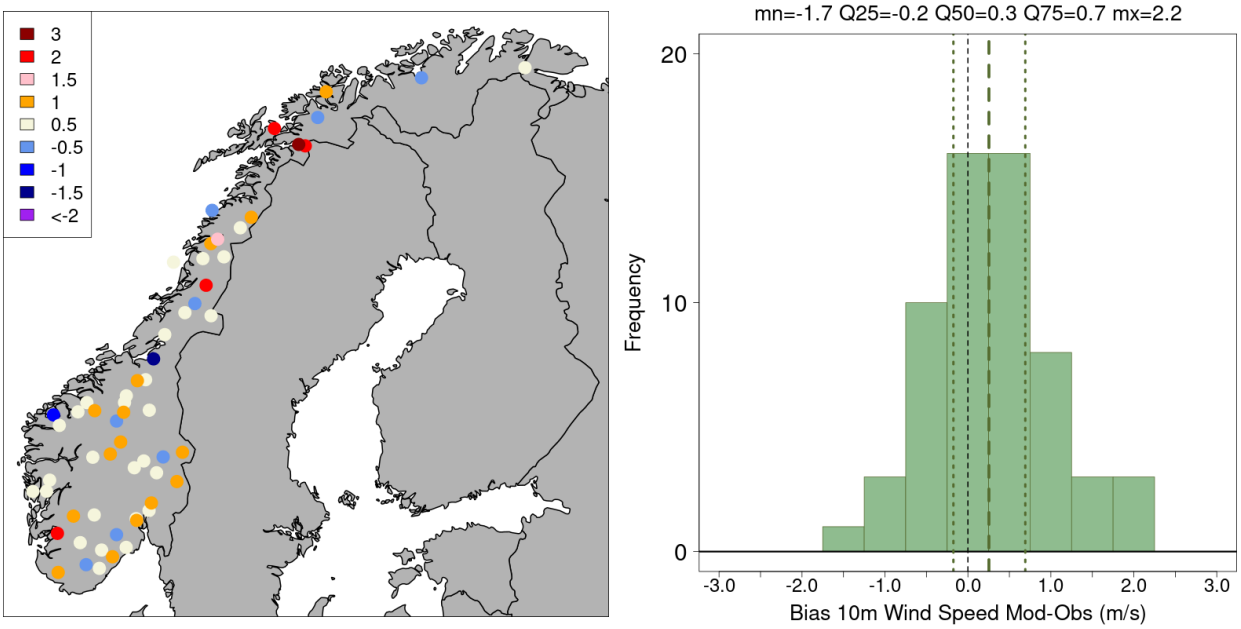


Figure 19: Mean error (or bias) of 10m hourly wind speed between modeled and observed data (Model minus Observations) for the period 2019–2023 across 74 stations. The modeled wind speed at each station location is calculated as the average from the nearest 4 grid points.

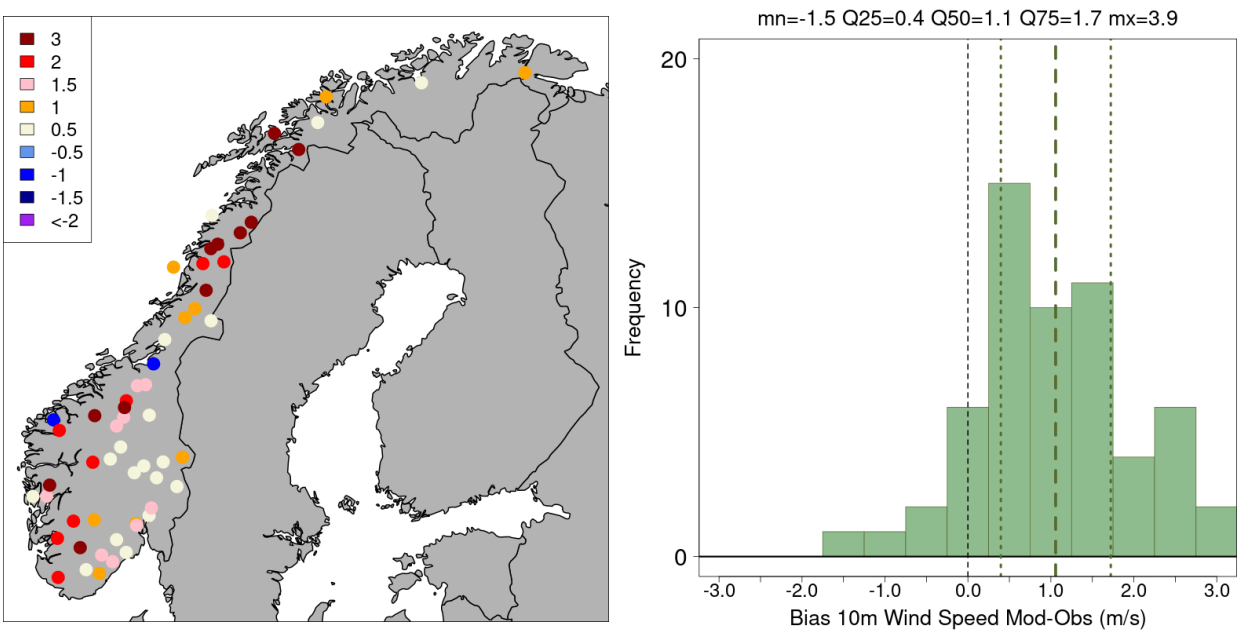


Figure 20: Mean error (or bias) of 10m hourly wind speed between modeled and observed data (Model minus Observations) for the period 2019–2023 across 74 stations. The modeled wind speed at each station location is calculated as the average from the nearest 200 grid points.

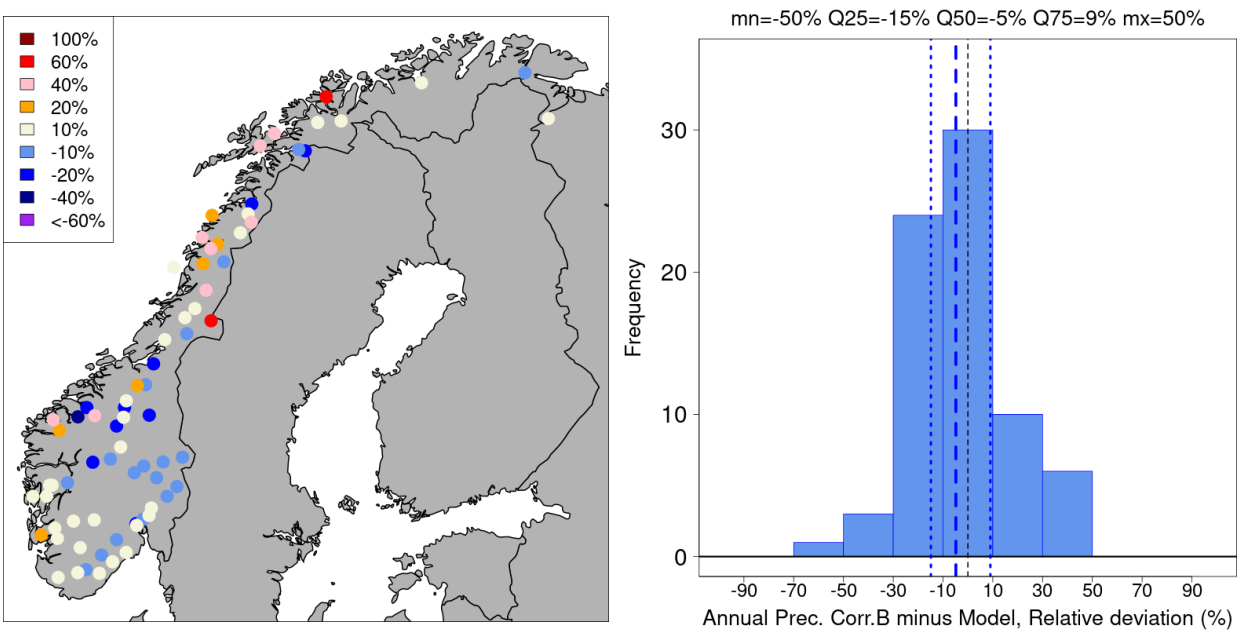


Figure 21: Comparison of corrected (using Correction B) and model-predicted mean annual total precipitation for the period 2019–2023 across 74 stations, with a focus on the relative deviation $D_k^{\mathrm{A}}/A_m$. For each observation and corresponding hour, the 10m wind speed from the model, employed in the correction, is derived as the average from the 4 nearest grid points. The maximum thresholds for the correction factor $k$ in Eq. 6 is set to 2. The layout is similar to Fig. 14.

| Correction | $\theta$ | $\beta$ | $\tau_1$ | $\tau_2$ | $T_\tau$ | $s_\tau$ |
|---|---|---|---|---|---|---|
| Correction A | 4.24 | 1.81 | 0.18 | 0.99 | 0.66 | 1.07 |
| Correction B | 3.41 | 1.58 | 0.18 | 0.99 | 0.69 | 1.15 |

Table 1: Parameters estimated for the adjustment function as proposed by *Wolff et al.* (2015), referenced here as Eq. (2). This table replicates Table 1 from *Wolff et al.* (2015), where only the optimal estimates are presented. Correction A pertains to parameters calculated with the 10m wind speed as input, whereas Correction B relates to parameters calculated using wind speed at gauge height.

| Class | Exposure | $k_l$ | $k_s$ |
|---|---|---|---|
| 1 | Extremely sheltered e.g. small clearing in the forest | 1.02 | 1.05 |
| 2 | Intermediate position between forest and plain | 1.05 | 1.10 |
| 3 | Relatively unsheltered location on a plain | 1.08 | 1.20 |
| 4 | Relatively unsheltered location in coastal or mountains region | 1.11 | 1.40 |
| 5 | Extremely unsheltered location in coastal or mountain region | 1.14 | 1.80 |

Table 2: Exposure correction factors ($k_l$ for liquid and $k_s$ for solid precipitation) used for production of daily seNorge precipitation maps.

| Station Name | Id | $\overline{A_m}$ (mm) | $\overline{D_g}$ (mm) | $\overline{D_k^{\mathrm{A}}}$ (mm) | $\overline{D_k^{\mathrm{B}}}$ (mm) |
|---|---|---|---|---|---|
| TRYSIL VEGSTASJON | 180 | 1173 | -210 (-18%) | -114 (-10%) | -162 (-14%) |
| HAKADAL JERNBANESTAS | 4460 | 1293 | -47 (-4%) | 40 (+3%) | -1 (-0%) |
| NORD-ODAL | 5350 | 963 | -163 (-17%) | -127 (-13%) | -142 (-15%) |
| FLISA II | 6020 | 818 | -174 (-21%) | -106 (-13%) | -137 (-17%) |
| RENA FLYPLASS | 7950 | 961 | -150 (-16%) | -108 (-11%) | -127 (-13%) |
| HJERKINN II | 9310 | 604 | -111 (-18%) | 151 (+25%) | 45 (+7%) |
| TYNSET - HANSMOEN | 9580 | 556 | -142 (-25%) | -105 (-19%) | -124 (-22%) |
| HAMAR - STAVSBERG | 12320 | 760 | -155 (-20%) | -101 (-13%) | -128 (-17%) |
| LILLEHAMMER - SÆTHER | 12680 | 1005 | -209 (-21%) | -161 (-16%) | -182 (-18%) |
| SKÅBU | 13655 | 685 | -44 (-6%) | 127 (+19%) | 38 (+6%) |
| DOVRE-LANNEM | 16400 | 771 | -339 (-44%) | -206 (-27%) | -272 (-35%) |
| OSLO - BLINDERN | 18700 | 1085 | -106 (-10%) | -35 (-3%) | -67 (-6%) |
| ASKER | 19710 | 1464 | -271 (-19%) | -167 (-11%) | -218 (-15%) |
| VEST-TORPA II | 21680 | 1135 | -244 (-21%) | -194 (-17%) | -218 (-19%) |
| BEITOSTØLEN II | 23550 | 1284 | -353 (-27%) | -44 (-3%) | -198 (-15%) |
| DRAMMEN - BERSKOG | 26900 | 1215 | -287 (-24%) | -237 (-20%) | -260 (-21%) |
| KONNERUD | 27010 | 1361 | -136 (-10%) | -23 (-2%) | -76 (-6%) |
| PORSGRUNN - ÅS | 30255 | 1158 | -59 (-5%) | 9 (+1%) | -16 (-1%) |
| MØSSTRAND II | 31620 | 1061 | -127 (-12%) | 338 (+32%) | 100 (+9%) |
| GVARV - NES | 32060 | 990 | -115 (-12%) | -94 (-9%) | -102 (-10%) |
| HAUKELISETER TESTFEL | 33950 | 1892 | -355 (-19%) | 1102 (+58%) | 537 (+28%) |
| GJERSTAD JERNBANESTA | 35210 | 1520 | -144 (-9%) | -73 (-5%) | -102 (-7%) |
| TVEITSUND | 37230 | 1310 | -159 (-12%) | -126 (-10%) | -139 (-11%) |
| HYNNEKLEIV | 38730 | 1531 | -164 (-11%) | -62 (-4%) | -108 (-7%) |
| BYGLANDSFJORD - NESE | 39750 | 1571 | -308 (-20%) | -257 (-16%) | -274 (-17%) |
| VALLE | 40250 | 1218 | 1 (+0%) | 29 (+2%) | 21 (+2%) |
| ÅSERAL | 41480 | 2129 | -65 (-3%) | 24 (+1%) | -11 (-1%) |
| EIK - HOVE | 43010 | 2750 | 152 (+6%) | 237 (+9%) | 220 (+8%) |
| GULLINGEN SKISENTER | 46220 | 3228 | -314 (-10%) | 621 (+19%) | 219 (+7%) |
| SAUDA | 46610 | 2711 | -149 (-5%) | -132 (-5%) | -134 (-5%) |

Table 3: Comparison of mean annual total precipitation across 74 stations. Here, $\overline{A_m}$ is the model prediction. $\overline{D_g}$ is the average difference between raw observations and model estimates. $\overline{D_k^{\mathrm{A}}}$ and $\overline{D_k^{\mathrm{B}}}$ are the average deviations between the model and observations corrected using Correction A and Correction B, respectively.

| Station Name | Id | $\overline{A_m}$ (mm) | $\overline{D_g}$ (mm) | $\overline{D_k^{\mathrm{A}}}$ (mm) | $\overline{D_k^{\mathrm{B}}}$ (mm) |
|---|---|---|---|---|---|
| VATS I VINDAFJORD | 46930 | 2421 | 200 (+8%) | 255 (+11%) | 245 (+10%) |
| KVAMSKOGEN - JONSHØG | 50310 | 3474 | -254 (-7%) | 136 (+4%) | -34 (-1%) |
| BERGEN - FLORIDA | 50540 | 2580 | 187 (+7%) | 261 (+10%) | 251 (+10%) |
| EVANGER | 51440 | 2219 | -111 (-5%) | -66 (-3%) | -80 (-4%) |
| BULKEN | 51470 | 1954 | 32 (+2%) | 167 (+9%) | 109 (+6%) |
| MJØLFJELL UH | 51800 | 2587 | -793 (-31%) | 254 (+10%) | -180 (-7%) |
| FILEFJELL - KYRKJEST | 54710 | 1285 | -575 (-45%) | -195 (-15%) | -363 (-28%) |
| STRYN - KROKEN | 58900 | 1681 | 150 (+9%) | 201 (+12%) | 179 (+11%) |
| ØRSTA - EITREFJELL | 59695 | 2121 | 351 (+17%) | 1456 (+69%) | 908 (+43%) |
| TAFJORD | 60500 | 2223 | -1166 (-52%) | -1082 (-49%) | -1121 (-50%) |
| MARSTEIN | 61420 | 2292 | -929 (-41%) | -811 (-35%) | -863 (-38%) |
| BJORLI | 61630 | 783 | 27 (+3%) | 624 (+80%) | 320 (+41%) |
| OPPDAL - SÆTER | 63705 | 793 | -150 (-19%) | 85 (+11%) | -38 (-5%) |
| DRIVDALEN | 63820 | 992 | -374 (-38%) | 71 (+7%) | -130 (-13%) |
| SOKNEDAL | 67280 | 1031 | 53 (+5%) | 268 (+26%) | 158 (+15%) |
| KOTSØY | 67560 | 1340 | -304 (-23%) | -157 (-12%) | -229 (-17%) |
| VÆRNES | 69100 | 1181 | -324 (-27%) | -275 (-23%) | -290 (-25%) |
| SNÅSA - KJEVLIA | 70850 | 1543 | -399 (-26%) | -101 (-7%) | -239 (-15%) |
| STEINKJER - SØNDRE E | 71000 | 1074 | -84 (-8%) | 25 (+2%) | -23 (-2%) |
| NORDLI - SANDVIKA | 73466 | 908 | 135 (+15%) | 816 (+90%) | 466 (+51%) |
| GARTLAND | 73550 | 1695 | -167 (-10%) | -15 (-1%) | -79 (-5%) |
| NAMSSKOGAN | 74350 | 1474 | 46 (+3%) | 200 (+14%) | 130 (+9%) |
| VEGA - VALLSJØ | 76450 | 1285 | -34 (-3%) | 162 (+13%) | 122 (+9%) |
| MOSJØEN LUFTHAVN | 77230 | 1449 | 104 (+7%) | 216 (+15%) | 171 (+12%) |
| MAJAVATN V | 77425 | 1364 | 100 (+7%) | 685 (+50%) | 409 (+30%) |
| SELJELIA | 78360 | 1655 | 153 (+9%) | 579 (+35%) | 387 (+23%) |
| VARNTRESK | 78800 | 1325 | -345 (-26%) | 11 (+1%) | -161 (-12%) |
| SKAMDAL | 79220 | 1679 | 70 (+4%) | 324 (+19%) | 225 (+13%) |
| HJARTÅSEN | 79764 | 1717 | -144 (-8%) | 94 (+5%) | -19 (-1%) |
| LURØY | 80200 | 2911 | 678 (+23%) | 1182 (+41%) | 1016 (+35%) |

Table 4: Continuation of Table 3

| Station Name | Id | $\overline{A_m}$ (mm) | $\overline{D_g}$ (mm) | $\overline{D_k^{\mathrm{A}}}$ (mm) | $\overline{D_k^{\mathrm{B}}}$ (mm) |
|---|---|---|---|---|---|
| REIPÅ | 80740 | 1636 | 46 (+3%) | 223 (+14%) | 165 (+10%) |
| SALTDAL - NORDNES | 81650 | 865 | -70 (-8%) | 37 (+4%) | -11 (-1%) |
| LØNSDAL STASJON | 81775 | 794 | -55 (-7%) | 577 (+73%) | 310 (+39%) |
| SETSÅ | 82000 | 1328 | -352 (-27%) | -225 (-17%) | -265 (-20%) |
| STRAUMSNES | 84500 | 1494 | -337 (-23%) | -48 (-3%) | -174 (-12%) |
| KATTERAT | 84880 | 1861 | -755 (-41%) | 8 (+0%) | -376 (-20%) |
| KANSTADBOTN | 85080 | 1829 | 408 (+22%) | 795 (+43%) | 624 (+34%) |
| HARSTAD STADION | 87640 | 894 | 72 (+8%) | 448 (+50%) | 284 (+32%) |
| BARDUFOSS | 89350 | 779 | -23 (-3%) | 133 (+17%) | 59 (+8%) |
| TAMOKDALEN | 89980 | 1547 | -353 (-23%) | 190 (+12%) | -91 (-6%) |
| TROMSØ | 90450 | 1084 | 254 (+23%) | 839 (+77%) | 571 (+53%) |
| ALTA LUFTHAVN | 93140 | 592 | -97 (-16%) | 57 (+10%) | -18 (-3%) |
| TANA BRU | 96850 | 610 | -155 (-25%) | 46 (+8%) | -59 (-10%) |
| NYRUD | 99540 | 578 | -96 (-17%) | 48 (+8%) | -26 (-4%) |

Table 5: Continuation of Table 3

# References


Bandhauer, M., F. Isotta, M. Lakatos, C. Lussana, L. Båserud, B. Izsák, O. Szentes, O. E. Tveito, and C. Frei (2022), Evaluation of daily precipitation analyses in e-obs (v19.0e) and era5 by comparison to regional high-resolution datasets in european regions, *International Journal of Climatology*, *42*(2), 727–747, doi:https://doi.org/10.1002/joc.7269.

Førland, E., P. Allerup, B. Dahlström, E. Elomaa, T. Jónsson, H. Madsen, J. Perälä, P. Rissanen, H. Vedin, and F. Vejen (1996), Manual for operational correction of nordic precipitation data, *DNMI report*, *24*, 96.

Haakenstad, H., Øyvind Breivik, B. R. Furevik, M. Reistad, P. Bohlinger, and O. J. Aarnes (2021), Nora3: A nonhydrostatic high-resolution hindcast of the north sea, the norwegian sea, and the barents sea, *Journal of Applied Meteorology and Climatology*, *60*(10), 1443 – 1464, doi:10.1175/JAMC-D-21-0029.1.

Haakenstad, H., and Øyvind Breivik (2022), Nora3. part ii: Precipitation and temperature statistics in complex terrain modeled with a nonhydrostatic model, *Journal of Applied Meteorology and Climatology*, *61*(10), 1549 – 1572, doi:10.1175/JAMC-D-22-0005.1.

Hersbach, H., B. Bell, P. Berrisford, S. Hirahara, A. Horányi, J. Muñoz-Sabater, J. Nicolas, C. Peubey, R. Radu, D. Schepers, A. Simmons, C. Soci, S. Abdalla, X. Abellan, G. Balsamo, P. Bechtold, G. Biavati, J. Bidlot, M. Bonavita, G. De Chiara, P. Dahlgren, D. Dee, M. Diamantakis, R. Dragani, J. Flemming, R. Forbes, M. Fuentes, A. Geer, L. Haimberger, S. Healy, R. J. Hogan, E. Hólm, M. Janisková, S. Keeley, P. Laloyaux, P. Lopez, C. Lupu, G. Radnoti, P. de Rosnay, I. Rozum, F. Vamborg, S. Villaume, and J.-N. Thépaut (2020), The era5 global reanalysis, *Quarterly Journal of the Royal Meteorological Society*, *146*(730), 1999–2049, doi:https://doi.org/10.1002/qj.3803.

Lavers, D. A., A. Simmons, F. Vamborg, and M. J. Rodwell (2022), An evaluation of era5 precipitation for climate monitoring, *Quarterly Journal of the Royal Meteorological Society*, *148*(748), 3152–3165, doi:https://doi.org/10.1002/qj.4351.

Michelson, D. B. (2004), Systematic correction of precipitation gauge observations using analyzed meteorological variables, *Journal of Hydrology*, *290*(3), 161–177, doi:https://doi.org/10.1016/j.jhydrol.2003.10.005.

Mohr, M. (2009), Comparison of versions 1.1 and 1.0 of gridded temperature and precipitation data for Norway, *Norwegian Meteorological Institute, met no note*, *19*.

Pollock, M. D., G. O'Donnell, P. Quinn, M. Dutton, A. Black, M. E. Wilkinson, M. Colli, M. Stagnaro, L. G. Lanza, E. Lewis, C. G. Kilsby, and P. E. O'Connell (2018), Quantifying and mit-

igating wind-induced undercatch in rainfall measurements, *Water Resources Research*, *54*(6), 3863–3875, doi:https://doi.org/10.1029/2017WR022421.

Reistad, M., Ø. Breivik, H. Haakenstad, O. J. Aarnes, B. R. Furevik, and J.-R. Bidlot (2011), A high-resolution hindcast of wind and waves for the north sea, the norwegian sea, and the barents sea, *Journal of Geophysical Research: Oceans*, *116*(C5).

Simmons, A. J., P. Berrisford, D. P. Dee, H. Hersbach, S. Hirahara, and J.-N. Thépaut (2017), A reassessment of temperature variations and trends from global reanalyses and monthly surface climatological datasets, *Quarterly Journal of the Royal Meteorological Society*, *143*(702), 101–119, doi:10.1002/qj.2949.

WMO-No.8 (2021), Wmo guide to meteorological instruments and methods of observation, *Tech. Rep. 8*, World Meteorological Organization.

Wolff, M. A., K. Isaksen, A. Petersen-Øverleir, K. Ødemark, T. Reitan, and R. Brækkan (2015), Derivation of a new continuous adjustment function for correcting wind-induced loss of solid precipitation: results of a norwegian field study, *Hydrology and Earth System Sciences*, *19*(2), 951–967, doi:10.5194/hess-19-951-2015.